This document is confidential and is proprietary to the American Chemical Society and its authors. Do not copy or disclose without written permission. If you have received this item in error, notify the sender and delete all copies.

Discovery of Novel Tacrine-Pyrimidone Hybrids as Potent Dual AChE/GSK-3 Inhibitors for the Treatment of Alzheimer's Disease

Journal:	*Journal of Medicinal Chemistry*
Manuscript ID	jm-2021-00160n.R3
Manuscript Type:	Article
Date Submitted by the Author:	n/a
Complete List of Authors:	Yao, Hong; China Pharmaceutical University Uras, Giuseppe; University of Nottingham, School of Pharmacy Zhang, Pengfei; China Pharmaceutical University Xu, Shengtao; China Pharmaceutical University Yin, Ying; China Pharmaceutical University Liu, Jie; China Pharmaceutical University Qin, Shuai; China Pharmaceutical University Li, Xinuo; University of Nottingham, School of Pharmacy Allen, Stephanie; University of Nottingham, School of Pharmacy Bai, Renren; Zhejiang University of Technology, College of Pharmaceutical Science Gong, Qi; Shanghai Institute of Materia Medica Chinese Academy of Sciences, CAS Key Laboratory of Receptor Research Zhang, Haiyan; Shanghai Institute of Materia Medica Chinese Academy of Sciences, CAS Key Laboratory of Receptor Research Zhu, Zheying; University of Nottingham, School of Pharmacy Xu, Jinyi; China Pharmaceutical University, Medicinal Chemistry

SCHOLARONE™
Manuscripts

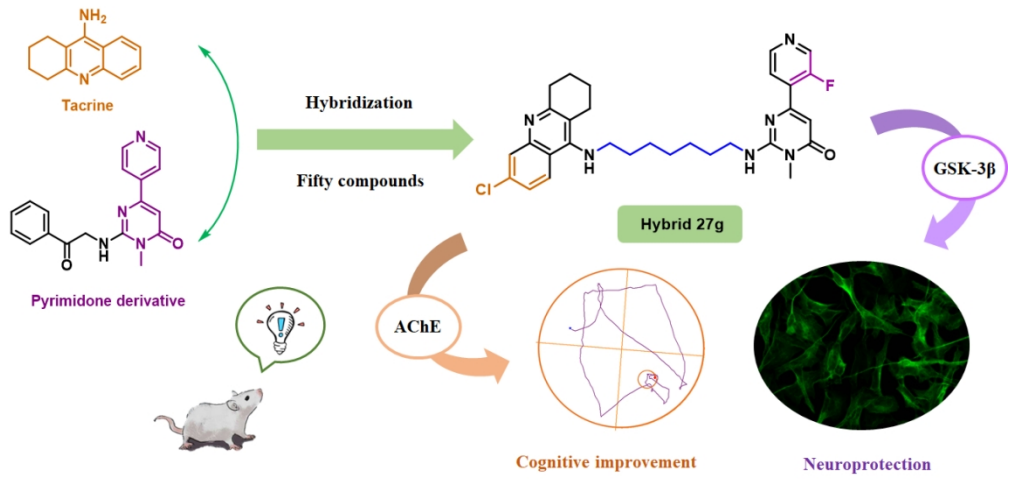
Tacrine
Pyrimidone derivative
Hybridization
Fifty compounds
Hybrid 27g
GSK-3β
AChE
Cognitive improvement
Neuroprotection

Discovery of Novel Tacrine-Pyrimidone Hybrids as Potent Dual AChE/GSK-3 Inhibitors for the Treatment of Alzheimer's Disease

Hong Yao,[†,#] Giuseppe Uras,[‡,#] Pengfei Zhang,[†,#] Shengtao Xu,[†] Ying Yin,[†,⊥] Jie Liu,[†] Shuai Qin,[†] Xinuo Li,[‡] Stephanie Allen,[‡] Renren Bai,[§] Qi Gong,[⊥] Haiyan Zhang,[⊥,*] Zheying Zhu,[‡,*] and Jinyi Xu[†,*]

[†]State Key Laboratory of Natural Medicines and Department of Medicinal Chemistry, China Pharmaceutical University, 24 Tong Jia Xiang, Nanjing, 210009, China

[‡]Division of Molecular Therapeutics & Formulation, School of Pharmacy, The University of Nottingham, University Park Campus, Nottingham NG7 2RD, UK

[§]College of Pharmacy, School of Medicine, Hangzhou Normal University, Hangzhou, 311121, China

[⊥]CAS Key Laboratory of Receptor Research, Shanghai Institute of Materia Medica, Chinese Academy of Sciences, 555 Zu Chong Zhi Road, Shanghai 201203, China

ABSTRACT

Based on a multi-target strategy, a series of novel tacrine-pyrimidone hybrids were identified for the potential treatment of Alzheimer's disease (AD). Biological evaluation results demonstrated that these hybrids exhibited significant inhibitory activities towards acetylcholinesterase (AChE) and glycogen synthase kinase 3 (GSK-3). The optimal compound **27g** possessed excellent dual AChE/GSK-3 inhibition both in terms of potency and equilibrium (AChE: IC_{50} = 51.1 nM; GSK-3β: IC_{50} = 89.3 nM), and displayed significant amelioration on cognitive deficits in scopolamine-induced amnesia mice, efficient reduction against phosphorylation of tau protein on Ser199 and Ser396 sites in glyceraldehyde (GA)-stimulated differentiated SH-SY5Y cells. Furthermore, compound **27g** exhibited eligible pharmacokinetic properties, good kinase selectivity and moderate neuroprotection against GA-induced reduction in cell viability and neurite damage in SH-SY5Y derived neurons. The multifunctional profiles of compound **27g** suggest that it deserves further investigation as a promising lead for the prospective treatment of AD.

INTRODUCTION

AD is a progressive neurodegenerative disorder with a currently incurable dementia syndrome; [1]

it afflicts millions of individuals globally in a chronic and fatal way.[2] The anatomical features of AD are extracellular senile plaques (SPs) and intracellular neurofibrillary tangles (NFTs) in the brain,[3] while the pathogenesis of AD is still inconclusive and undefined since it was first reported by Alois Alzheimer in 1907.[4] Accumulated research data have confirmed that the progression of AD is mainly evident in cholinergic deficits,[5] tau protein hyperphosphorylation,[6] β-amyloid (Aβ) aggregation,[7] oxidative damage,[8] unbalanced homeostasis of biometals,[9] glutamate-related excitotoxicity,[10] serotonergic dysfunction,[11] histaminergic dysfunction,[12] and reduced signal transduction mediated by second messengers.[13] The present anti-AD therapies rationally regulate key targets in related signaling pathways, which could be classified as single-target strategies and multitarget strategies.[14] Approved drugs based on a single target (Fig. 1A) show obvious improvements in cognition and memory in clinical applications,[15] but the progression of AD cannot be stopped or reversed by these drugs because of the compensatory effects of other morbid signaling pathways. In consideration of the complicated interrelation among multiple pathways, a multitarget strategy possesses a more effective and promising capacity to manage the special disease network of AD with synergistic adjustment towards more pivotal targets, becoming a hot research topic for the potentially curable treatment of AD.[16]

The cholinergic hypothesis, a classical theory in AD pathology proposed in 1976,[17] states that the neurotransmitter acetylcholine (ACh) in the hippocampus and the neocortex regions plays a key role in learning and memory,[18] and the remarkable decline in the level of ACh is primarily responsible for the dementia of AD patients. Under physiological conditions, acetylcholinesterase (AChE) can hydrolyze ACh to choline and acetate with high efficiency.[19] Thus, inhibition against AChE is an advisable way to enhance the concentration of ACh in the synaptic cleft, making it a crucial target in the cholinergic system. Drugs approved by the FDA for the treatment of AD have demonstrated the therapeutic value of AChE, among which donepezil (**1**), galantamine (**2**), rivastigmine (**3**), tacrine (**4**), and huperzine A (**5**, approved by CFDA) are all AChE inhibitors (AChEIs) (Fig. 1A).[20] In addition, appropriate AChEIs could inhibit the oligomerization and fibrillization of Aβ induced by AChE,[21,22] indicating the multifunctional profiles of AChEIs in potential anti-AD therapy.

Meanwhile, the tau protein hypothesis is another significant inference regarding AD pathology, stating that microtubule depolymerization and NFT generation, which are mostly caused by tau protein hyperphosphorylation, accelerate the degeneration and necrosis of neuronal cells, resulting

in the progressive deterioration of disease conditions.[6] Disordered phosphorylation of tau protein catalyzed by glycogen synthase kinase 3 beta (GSK-3β), primarily at Ser396, Ser199, and Ser404 sites,[23] increases the number of additional 2-7 phosphate groups and weakens its adhesion with microtubules. Subsequently, hyperphosphorylated tau protein separates from microtubules and aggregates into insoluble NFTs, leading to instability of the microtubule structure and ultimately cell death.[24] Therefore, GSK-3β upstream of the tau protein signaling pathway has become a vital target for new anti-AD drug design,[25] and its inhibition could directly benefit the microtubule system and reduce intracellular NFTs, as well as radiate to Aβ signaling pathways by reducing the formation of Aβ.[26]

The cholinergic signaling pathway has a close connection with the tau protein signaling pathway in AD pathogenesis. Evidence has shown that the neuroprotective mechanism of AChEI donepezil (**1**) is related to the inactivation of GSK-3β[27] and further induces a corresponding decrease in the insolubility and hyperphosphorylation of tau protein.[28] On the other hand, phosphorylated tau protein (p-Tau) can trigger highly upregulated expression of AChE, which would consequently lead to suppression of the cholinergic system, and initially, increased levels of AChE around NFTs would result in disturbing tau phosphorylation.[29] Thus, simultaneous modulation targeting AChE and GSK-3β has mutually beneficial effects for the amelioration of both cholinergic and tau protein signaling pathways, and new chemical entities (NCEs) with dual AChE/GSK-3β inhibition have promising potential to improve AD conditions through multiple regulatory mechanisms, such as ACh enhancement, NFT reduction, and Aβ suppression. However, related anti-AD studies based on AChE/GSK-3β targets are rare.[30,31,32] To broaden research on multifunctional anti-AD drugs, the discovery of novel and promising lead compounds with multiple anti-AD properties is extremely urgent.

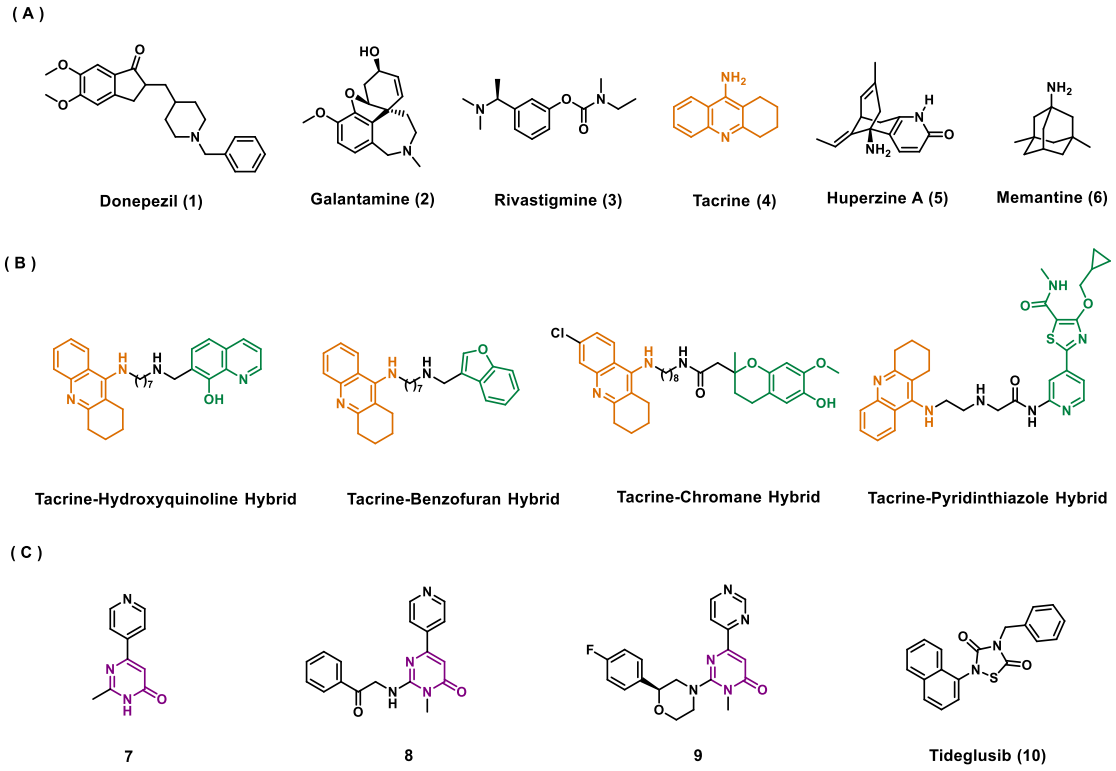

Figure 1. (A) Drugs approved by FDA or CFDA for the treatment of AD. (B) Representative hybrids bearing tacrine unit as anti-AD agents through multiple regulatory mechanisms. (C) The structures of several typical GSK-3*β* inhibitors.

Tacrine (**4**) (Fig. 1A) was the first AChEI drug approved in 1993, but it was regretfully withdrawn by the FDA due to liver toxicity.[1] Evidence has shown that the structure of **4** is still popular in anti-AD studies, especially in multitarget related studies.[33] For example (Fig. 1B), tacrine-hydroxyquinoline hybrid[34] exhibited both AChE inhibitory activity and metal chelating ability, a tacrine-benzofuran hybrid[35] was proven to be a dual inhibitor targeting AChE and *β*-site amyloid precursor protein cleaving enzyme (BACE-1), a tacrine-chromane hybrid[36] was found to exert multiple AChE inhibition and antioxidative effects, and a tacrine-pyridinthiazole hybrid was recently found to possess AChE and GSK3β dual inhibition activities.[32] Therefore, the unique three-ring pharmacophore of **4** was used in our design of new anti-AD hybrids.

Compound **7** is a typical GSK-3*β* inhibitor, and further modification on its pyrimidone moiety offered derivative **8** bearing more potent inhibitory activity towards GSK-3*β* (Fig. 1C).[37] Subsequent optimization on substituent groups of pyrimidone scaffold offered compound **9**,[38] which showed

similar high affinity for GSK-3β and better pharmacokinetic profiles than compound **8** (Fig. 1C). Indeed, the pyrimidone unit is the key pharmacophore of the above compounds exerting GSK-3β inhibition. Given the significance of pyrimidone for druggability[39] and the possible GSK-3β inhibitory activity of its derivatives, the structure of pyrimidone was also used as a pivotal moiety in our design of NCEs for anti-AD.

As shown in Fig. 2, the tacrine moiety of hybrids was principally designed to retain AChE inhibition, the structure of aromatic ring-substituted pyrimidone was applied to maintain potential GSK-3β inhibition, and the alkylamine linker was selected as an appropriate bridge to realize the incorporation of the two pharmacophores above. Furthermore, the hybrids underwent fine-tuning of structures to obtain a better target binding effect. For example, in the case of AChE inhibition, the substitution patterns of the tacrine unit leading to optimal cholinesterase inhibition are very well known, with higher potencies observed when halogen atoms or methyl groups are introduced into position at C6.[36] Therefore, the substitution patterns of tacrine moiety is worth investigating. In addition, the introduction of the linker and pyrimidone moiety into the tacrine might form a new interaction with AChE, so the linker and pyrimidone moiety should be slightly modified to maintain or enhance AChE inhibition. Herein, we have identified a novel series of dual AChE/GSK-3β inhibitors by fusing the key skeletons of tacrine (**4**) and pyrimidone (**8**) based on the multitarget anti-AD strategy, aiming to alleviate cholinergic deficits and synergistically eliminate intracellular NFTs. These hybrids underwent two iterative cycles of optimization, and abundant pharmacological experiments were performed to investigate their drug-like properties, which provided optimistic feedback. Through effective regulation of both cholinergic and tau protein signaling pathways, we envisaged that such promising tacrine-pyrimidone hybrids could exhibit favorable effects under real disease conditions of AD, offering valuable information for the development of anti-AD therapies.

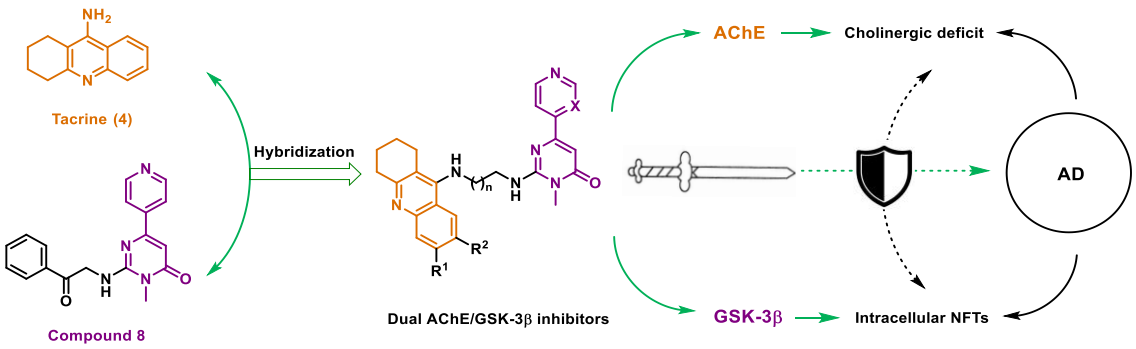

Figure 2. Design strategy of tacrine-pyrimidone hybrids with dual AChE/GSK-3β inhibition

RESULTS AND DISCUSSION

Design and synthesis

First, the tacrine moiety of the novel scaffold of hybrids was investigated mainly for potential AChE inhibition. Since higher AChE inhibition potencies are observed when halogen atoms or methyl groups are introduced to the phenyl ring of tacrine,[36] the substituent of the phenyl moiety was investigated. As depicted in Scheme 1 and Scheme S1, starting material **11a** was treated with *N*,*N'*-carbonyldiimidazole (CDI) and ethyl potassium malonate to produce **12a**. Cyclization of **12a** with *N*-methylthiourea and successive chlorination by $POCl_3$ afforded the key intermediate **14a**.[37] Esters with different substituents (**15**), another kind of starting material, were treated with NaOH to provide carboxylic acid (**16**), which underwent cyclization with cyclohexanone to achieve three-ring structures (**17**). Subsequently, the corresponding diamines were attached to **17** under the catalysis of NaI to form key intermediates **18a-m**,[30] which were coupled with **14a** under alkaline conditions to yield hybrids **21a-m** with diverse substituents (series 1).

Second, the pyrimidone moiety of the novel scaffold of hybrids was investigated mainly for potential GSK-3*β* inhibition. It was found that the introduction of a fluorine atom or the change of pyridine by a pyrimidine ring linked to the pyrimidone moiety would be beneficial for binding with GSK-3β,[37,38,40] therefore, compound **14a-c** were synthesized as described in Scheme 1. Compared with **14a**, key intermediates **14b-c** were synthesized from starting materials **11b-c** similarly.[38,40] Then, **14b-c** were treated with corresponding intermediates from **18a-m** in the presence of K_2CO_3 to yield target compounds **22a-j** (series 2).

Third, the linker of the novel scaffold was investigated mainly for balanced dual inhibition against AChE/GSK-3*β,* as depicted in Scheme 1. Key intermediates **19a-e** were prepared by amination of compound **17a** with diverse diamines in the presence of NaI, and the subsequent condensation reaction with **14a** in tetrahydrofuran (THF) solvent produced hybrids **23a-e** (series 3).

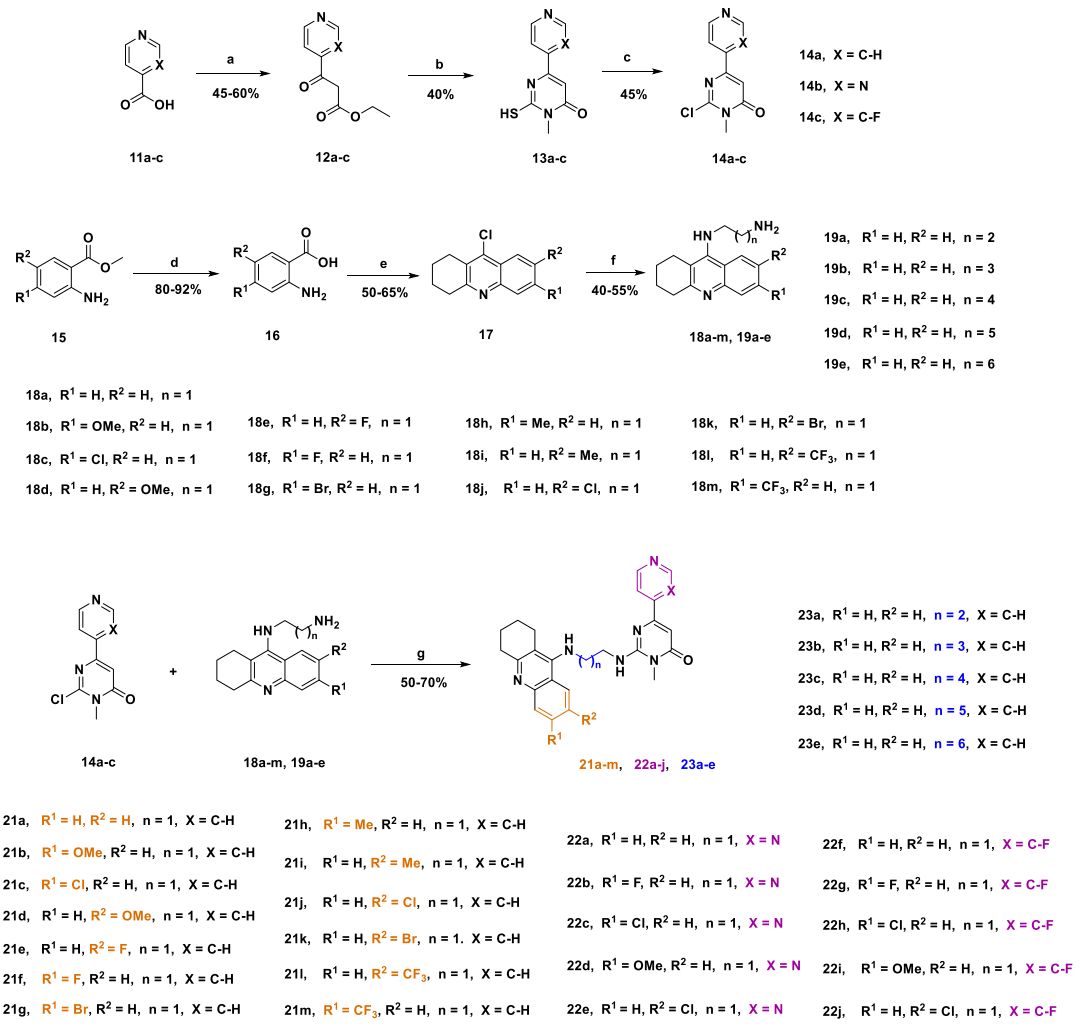

Scheme 1. Synthesis of key intermediates **14a-c**, **18a-m**, and **19a-e**, and final hybrids **21a-m**, **22a-j**, and **23a-e**. Reagents and conditions: (a) (i) *N*,*N*'-carbonyldiimidazole, dry THF, reflux, 1-2 h; (ii) ethyl potassium malonate, $MgCl_2$, dry THF, reflux, overnight; (b) *N*-methylthiourea, DBU, EtOH, reflux, overnight; (c) $POCl_3$, DMF, 1,2-dichloroethane, 65 °C, 1 h; (d) (i) 2 N NaOH, r.t., overnight; (ii) conc. HCl, r.t., 10 min; (e) cyclohexanone, $POCl_3$, 115 °C, 3-5 h; (f) corresponding diamine, NaI, *n*-pentanol, reflux, 12-24 h; (g) K_2CO_3, THF, reflux, overnight.

The first round of evaluation of the dual AChE/GSK-3β inhibitory potency of compounds in series 1-3 confirmed our design strategy and provided explicit guidance for further optimization of hybrids (Table 1). Thus, in the fourth modification, more promising compounds were designed and synthesized by assembling the positive building blocks confirmed by series 1-3, as described in Scheme 2. Key intermediates **24a-e** or **25a-e** were obtained from the amination of relative compound **17** using 1,6-heptanediamine or 1,7-hexanediamine agents in the presence of NaI. Then, key intermediates **14a** and **14c** were adopted to react with **19d-e**, **24a-e**, or **25a-e**, giving

corresponding target compounds **26a-k** (series 4) and **27a-k** (series 5), which underwent the second round of evaluation of dual AChE/GSK-3*β* inhibitory activities soon after (Table 2).

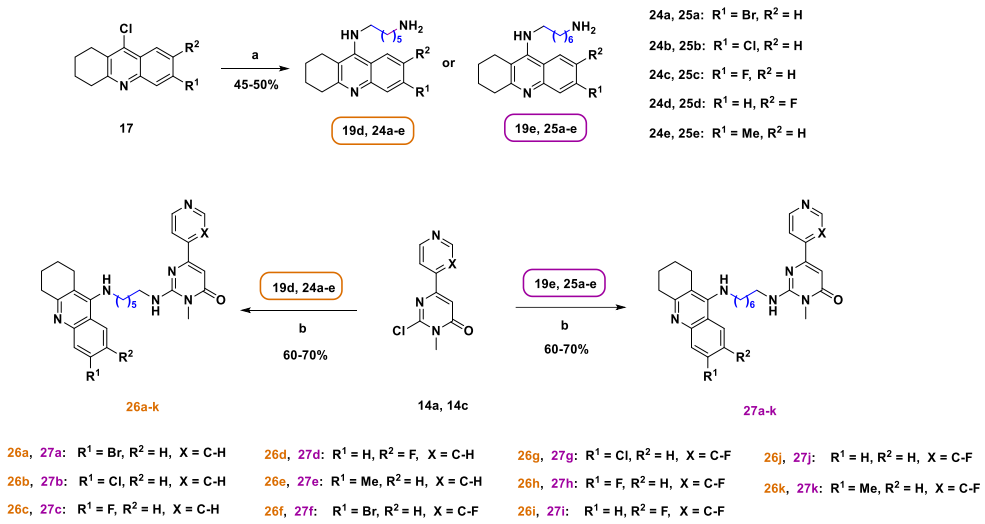

Scheme 2. Synthesis of key intermediates **24a-e**, **25a-e**, and final hybrids **26a-k**, **27a-k**. Reagents and conditions: (a) 1,7-heptanediamine or 1,6-hexanediamine, NaI, *n*-pentanol, reflux, 12-24 h; (b) K_2CO_3, THF, reflux, overnight.

In total, fifty derivatives in five series (i.e., **21a-m**, **22a-j**, **23a-e**, **26a-k**, and **27a-k**) were designed and synthesized. Related details of the synthetic procedures and structural characterization of key intermediates and target compounds are described in the Experimental Section and Supporting Information.

In vitro AChE and GSK-3*β* inhibitory activities

In the first round of biological evaluation, the inhibitory potency of compounds **21a-m** (series 1), **22a-j** (series 2) and **23a-e** (series 3) towards AChE/GSK-3*β* was assessed *in vitro*. The commercially available compounds donepezil (**1**), tacrine (**4**) and AR-A014418[41] were used as positive controls for AChE and GSK-3*β*, respectively. Since the high homology between the murine and human AChE enzymes (with identities of 89%), and the consistent IC50 data obtained with reference compounds (huperzine A[42], huperzine B[43] and donepezil (Table S1)) across the two species in our previous studies, and therefore, a murine AChE-based screening was applied in the current study. The inhibition against two targets of all compounds at 1.0 μM was tested in primary screening, and compounds with favorable results were further measured to obtain their IC_{50} values, which are

presented in Table S2 and Table 1.

Compounds **21a-m** and **22a-j** had poor to good inhibitory activity against AChE (0.16 μM to 23 μM, Table 1), suggesting that substituent groups in both of the tacrine moiety and pyrimidine moiety were important for the inhibition of AChE (see in supporting information for more details of the discussion of inhibitory activity against AChE). It was found that substituent groups in the R^1 site had better inhibitory activity than the same group in the R^2 site (see **21g** vs **21k**, **21c** vs **21j**, **21h** vs **21i**, **21b** vs **21d**, and **21m** vs **21l** in Table 1), and compounds with halogen groups (Br-/Cl-/F-) in the R^1 site and fluorine in the R^2 site were beneficial for anti-AChE activity. However, none of them had sufficient inhibitory potency against GSK-3β (Table 1). Although the biological data were not sufficient in the series of 1-2, pyrimidone with an F-substituted pyridine group (X = C-F) demonstrated its ability to inhibit GSK-3β (Table 1), which was adopted in posterior design. Meanwhile, although pyridine-substituted pyrimidone (X = C-H) had similar potency with imidazole-substituted pyrimidone (X = N), the structure containing X = C-H was chosen as a representative core for further study along with the core containing X = C-F, since the potency of **21a** was slightly better than **22a** (Table 1).

The alkylamine linker between the tacrine unit and pyrimidone unit was studied in the compound series of 3 (**23a-e**) with the length of the carbon chain changed from three (n = 2) to seven (n = 6). Among the novel compounds in series 3, hybrid **23d** (n = 5) had the best IC_{50} value of 0.12 μM against AChE. Compound **22h** (n = 1), the best AChE inhibitor in series 1-2, had an IC_{50} value of 0.16 μM. Thus, along with the increase in carbon chains, the inhibitory potency of compounds towards AChE increased. For the target GSK-3β, compound **22f** (n = 1) was the best inhibitor with an IC_{50} value of 1.18 μM in series 1-2, and novel hybrid **23e** (n = 6) had more favorable potency with an IC_{50} value of 0.33 μM. Therefore, the GSK-3β inhibition of hybrids increased in a major way along with the increase of the carbon chain, suggesting that the short carbon chain of compounds in series 1-2 (**21a-m** and **22a-j**) limited the capacity of pyrimidone moiety binding to enzyme GSK-3β. In addition to the enhanced potency, a favorable balance of inhibition against two targets was also achieved when the alkyl chain had six or seven carbon atoms. Considering that **23d-e** were the most promising dual AChE/GSK-3β inhibitors among the compound series 1-3, **23d** (IC_{50} = 0.12 μM for AChE, IC_{50} = 0.52 μM for GSK-3β) had better AChE inhibition and weak GSK-3β inhibition than **23e** (IC_{50} = 0.13 μM for AChE, IC_{50} = 0.33 μM for GSK-3β), and alkylamine

linkers with six or seven carbon atoms were both adopted for further exploration. Additionally, hybrids holding alkyl alcohol linkers were designed, synthesized (Scheme S2) and evaluated in our work with positive feedback, and the alkyl alcohol linker was abandoned in our further research because its integral results on dual inhibition had a slightly inferior effect than the alkylamine linker (Supporting Information, Table S3).

Table 1. Structures and Inhibitory Activities towards AChE and GSK-3β of Compounds **21a-m**, **22a-j**, and **23a-e**

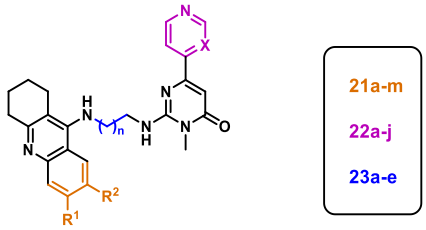

Compd.	R^1	R^2	n	X	IC_{50} (μM) ± SEM[a]	
					AChE[b]	GSK-3β[c]
21a	H	H	1	C-H	1.06 ± 0.21	4.04 ± 0.06
21b	OMe	H	1	C-H	8.30 ± 0.28	-[d]
21c	Cl	H	1	C-H	0.49 ± 0.04	-[d]
21d	H	OMe	1	C-H	15.7 ± 1.35	-[d]
21e	H	F	1	C-H	0.37 ± 0.01	-[d]
21f	F	H	1	C-H	3.90 ± 0.15	-[d]
21g	Br	H	1	C-H	0.44 ± 0.07	-[d]
21h	Me	H	1	C-H	1.89 ± 0.45	-[d]
21i	H	Me	1	C-H	20.0 ± 2.40	-[d]
21j	H	Cl	1	C-H	10.9 ± 1.37	-[d]
21k	H	Br	1	C-H	15.8 ± 0.54	-[d]
21l	H	CF_3	1	C-H	-[d]	-[d]
21m	CF_3	H	1	C-H	11.3 ± 0.79	-[d]
22a	H	H	1	N	0.80 ± 0.01	5.63 ± 0.16
22b	F	H	1	N	0.18 ± 0.00	-[d]

22c	Cl	H	1	N	0.42 ±0.01	- [d]
22d	OMe	H	1	N	23.0 ±0.29	- [d]
22e	H	Cl	1	N	18.8 ±0.18	- [d]
22f	H	H	1	C-F	4.98 ±0.18	1.18 ±0.03
22g	F	H	1	C-F	0.73 ±0.08	11.9 ±0.95
22h	Cl	H	1	C-F	0.16 ±0.00	14.0 ±1.35
22i	OMe	H	1	C-F	9.92 ±0.99	19.0 ±1.90
22j	H	Cl	1	C-F	9.80 ±0.35	8.13 ±0.60
23a	H	H	2	C-H	2.85 ±0.11	- [d]
23b	H	H	3	C-H	1.42 ±0.06	0.92 ±0.02
23c	H	H	4	C-H	0.40 ±0.02	1.28 ±0.04
23d	H	H	5	C-H	**0.12 ±0.01**	**0.52 ±0.01**
23e	H	H	6	C-H	**0.13 ±0.01**	**0.33 ±0.01**
Tacrine (**4**)					0.20 ±0.01	>100
Donepezil (**1**)					6.1 ±0.3 nM	>100
AR-A014418[e]					>40	0.49 ±0.04

[a]Data are expressed as the mean of three independent determinations. [b]The zymogen of AChE was from the cerebral cortex of mouse. [c]Recombinant human GSK-3β was used. [d]The inhibitory activities of compounds were not favorable at primary screening (inhibitory effect less than 50% at 1 μM), of which the IC_{50} values were not further tested. [e]A typical GSK-3β inhibitor used as the positive control.

In short, the first round of evaluation of compounds from series 1-3 (**21a-m**, **22a-j**, **23a-e**) showed that halogen groups (Br-/Cl-/F-) as substituent R^1, fluorine as substituent R^2, a longer alkyl linker (n = 5 or 6), and pyridine-substituted (X = C-F or C-H) pyrimidone were more beneficial for dual AChE/GSK-3β inhibition of compounds. Therefore, hybrids based on the above building blocks were further designed and synthesized as series 4 (**26a-k**) and series 5 (**27a-k**), and their dual AChE/GSK-3β inhibitory activities were assessed *in vitro* (Table 2). In the same way, the typical AChEI donepezil (**1**) and GSK-3β inhibitor AR-A014418 were used as corresponding positive controls in the second round of biological evaluation. In particular, only the IC_{50} values of compounds that exhibited potent inhibition at 1.0 μM in primary screening were measured for the

GSK-3β target.

From the perspective of AChE inhibition, the positive results of compound series 4-5 (**26a-k** and **27a-k**) could possibly be ascribed to tacrine units bearing diverse substituents. Compared to substituent R^2, the fluoro group of R^1 showed superiority without controversy in hybrids bearing longer alkyl tethers (**26c** vs **26d**, **26h** vs **26i**, **27c** vs **27d**, and **27h** vs **27i**). Halogen groups Br- and Cl- were more powerful for enhancing AChE inhibition, with IC_{50} values of **26a-b**, **26f-g**, **27a-b**, and **27f-g** lower than 100 nM, constituting the first level of inhibitor echelon. Furthermore, **27a-b** and **27f-g,** bearing seven carbon atoms in the linker, possessed more potent activities than **26a-b** and **26f-g**, respectively, of which **27b** was the most effective AChE inhibitor with an IC_{50} value of 37.5 nM. It is interesting to note that in the compound series of 4-5 (**26a-k** and **27a-k**), only the introduction of Br and Cl groups to the tacrine unit (**26a-b**, **26f-g**, **27a-b**, and **27f-g**) could further enhance the inhibitory activity of new compounds compared to **23d,** which had the best AChE inhibition among the series 1-3 in the first round of biological evaluation.

From the perspective of GSK-3β inhibition, the objective results of series 5 indicated that the pyrimidone unit bearing fluorine-substituted pyridine (X = C-F) was the pivotal pharmacophore to obtain stronger affinity with the enzyme, and the pyridine-substituted pyrimidone moiety (X = C-H) was relatively weak. Changing groups in the tacrine units of hybrids had a minor influence on the inhibitory activities against GSK-3β, while alkylamine linkers with more carbon atoms could increase GSK-3β inhibition (**27f-k**) compared to compounds **26f-k** (series 4). In series 5, hybrids **27f-g** and **27i-j** belonged to the first level of the inhibitor group with IC_{50} values lower than 100 nM, of which **27j** was the most potent GSK-3β inhibitor (IC_{50} = 67.2 nM).

The results from the second round were successful and valuable, confirming the speculation from the first round and further clarifying the value of alternative building blocks, such as the fluorine group in R^1 or R^2, the type of X in the pyrimidone unit, and the length of the alkyl chain for the linker. Remarkably, the seven-carbon alkyl linker made an outstanding contribution to the hybrids to achieve a favorable inhibitory balance towards AChE/GSK-3β, which is an important factor in administration dosage and *in vivo* toxicity aspects. Thus, hybrids **23d**, **23e**, **26h**, **26k**, **27f**, **27g**, **27h**, and **27k** possessed excellent inhibitory equilibrium and activities and could be considered as promising dual AChE/GSK-3β inhibitors for further study to find new potential treatments for AD; of these, **23e** (IC_{50} = 0.13 μM for AChE, IC_{50} = 0.33 μM for GSK-3β) is the representative hybrid

among series 1-3, and **27g** (IC_{50} = 51.1 nM for AChE, IC_{50} = 89.3 nM for GSK-3β) is the optimal compound among series 1-5.

In summary, for the novel scaffold fused from tacrine and pyrimidone, the introduction of halogen groups Br- and Cl- as substituents of R^1 of the tacrine unit is very favorable for AChE inhibition, pyrimidone units bearing fluorine-substituted pyridine groups are the best pharmacophores towards the GSK-3β target, and alkylamine linkers with a linear chain of seven carbons are the most beneficial moiety for inhibitory balance.

Table 2. Structures and Dual AChE/GSK-3β Inhibitory Activities of Compounds **26a-k** and **27a-k**

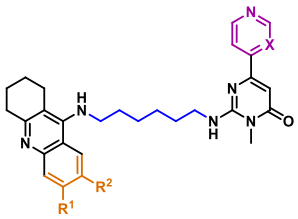

26a-k

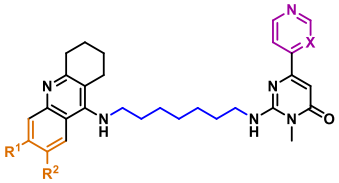

27a-k

Compd.	R^1	R^2	X	IC_{50} (nM) ±SEM[a]	
				AChE[b]	GSK-3β[c]
26a	Br	H	C-H	45.0 ±2.2	-[d]
26b	Cl	H	C-H	53.0 ±3.0	-[d]
26c	F	H	C-H	163.3 ±10.5	-[d]
26d	H	F	C-H	2417 ±239.0	-[d]
26e	Me	H	C-H	238.7 ±16.4	-[d]
26f	Br	H	C-F	70.3 ±3.3	178.7 ±17.9
26g	Cl	H	C-F	52.7 ±6.2	178.0 ±8.5
26h	F	H	C-F	134.3 ±8.5	174.3 ±2.7
26i	H	F	C-F	2210 ±135.8	153.7 ±8.9
26j	H	H	C-F	631.0 ±35.2	126.3 ±2.2
26k	Me	H	C-F	298.3 ±7.5	238.7 ±22.3
27a	Br	H	C-H	39.0 ±3.0	-[d]
27b	**Cl**	H	C-H	**37.5 ±4.0**	-[d]
27c	F	H	C-H	123.7 ±3.5	-[d]

27d	H	F	C-H	1800 ±104.4	- [d]
27e	Me	H	C-H	145.0 ±4.0	- [d]
27f	Br	H	C-F	58.1 ±5.2	91.0 ±7.0
27g	**Cl**	H	**C-F**	**51.1 ±4.6**	**89.3 ±0.1**
27h	F	H	C-F	134.3 ±7.9	103.7 ±9.0
27i	H	F	C-F	2380 ±193.0	96.1 ±2.7
27j	H	H	**C-F**	352.0 ±21.4	**67.2 ±4.7**
27k	Me	H	C-F	174.3 ±10.2	137.0 ±20.0
Tacrine (**4**)				202.1 ±12.5	$>10^5$
Donepezil (**1**)				9.8 ±0.7	$>10^5$
AR-A014418[e]				$>4*10^4$	492.0 ±41.7

[a]Data are expressed as the mean of three independent determinations. [b]The zymogen of AChE was from the cerebral cortex of mouse. [c]Recombinant human GSK-3β was used. [d]The inhibitory activities of compounds were relatively not potent enough at primary screening (inhibitory effect less than 60% at 1 μM). Under comprehensive consideration, the exact IC_{50} values of them were not detected. [e]A typical GSK-3β inhibitor used as a positive control.

Molecular modeling

As the most promising compound after two rounds of design, **27g** (IC_{50} = 51.1 nM for AChE, IC_{50} = 89.3 nM for GSK-3β) exhibited a notable increase in inhibitory potency against dual targets compared with the representative hybrid **23e** (IC_{50} = 0.13 μM for AChE, IC_{50} = 0.33 μM for GSK-3β) from the first round of design. To gain insights into the binding patterns with the AChE and GSK-3β enzymes responsible for the difference in activities, molecular docking studies were performed using Schrodinger Glide (Figure S1). The docking results are shown in Figures 3-4 and Figures S2-S3 after preparation by PyMOL.

As shown in Figure 3, both compounds **23e** and **27g** could occupy the catalytic anionic site (CAS) and the peripheral anionic site (PAS) of AChE, of which the tacrine units were located in the interior of the AChE gorge, and pyrimidone fragments were located in the exterior of the AChE gorge, forming the foundation of AChE inhibition (Fig. 3A/B). The specific orientation of **23e** and **27g** in the binding pocket was evident, resulting in different binding patterns and corresponding inhibitory potency (Fig. 3C/D). There were only two π-π stacking contacts between **23e** and Trp-86, while

there were five secondary bonds between **27g** and the binding gorge mainly due to the introduction of Cl- groups on the tacrine unit. Compared with **23e**, the hydrogen bond (3.5 Å) between the chlorine of **27g** and oxygen of Tyr-72 propels the reversal of the tacrine unit, losing one π-π stacking contact with Trp-86, inducing two more π-π stacking contacts with Trp-286 and one more hydrogen bond with Ser-293 (2.2 Å) for the pyrimidone unit through the relay of the alkyl linker. Halogen bonds frequently occur in the presence of chlorine or bromine, which are large enough to contain σ-holes,[44] meaning that it is difficult for tacrine units bearing fluorine groups to form halogen bonds with Tyr-72. Thus, the docking results of AChE were consistent with the structure-activity relationships (SARs) of hybrids.

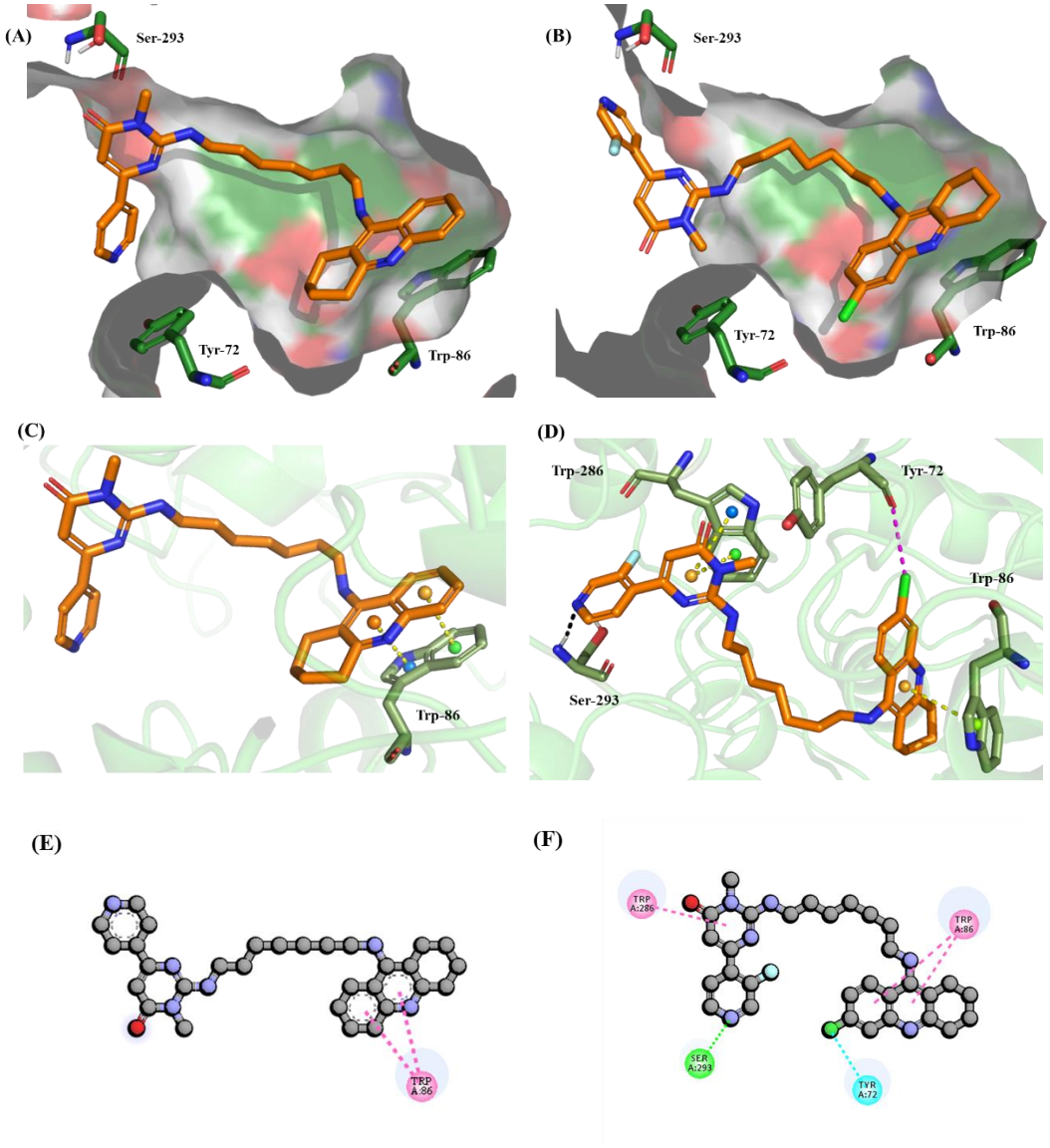

Figure 3. Proposed binding models of **23e** (A/C) or **27g** (B/D) with AChE (PDB code: 4EY7). For secondary bonds,

hydrogen bond was shown as black dotted line, halogen bond was shown as a pink dotted line, π-π stacking contacts were shown as yellow dotted lines. (A) The relative position of compound **23e** (shown in brown) in the active pocket of AChE. (B) The relative position of **27g** (shown in brown) in the active pocket of AChE. (C) Interactions between **23e** (shown in brown) and amino acid residue of AChE. (D) Interactions between **27g** (shown in brown) and amino acid residue of AChE. (E) The 2D binding mode of compound **23e** with AChE, the π-π stacking contact was shown as purple. (F) The 2D binding mode of compound **27g** with AChE, the π-π stacking contacts were shown as purple, the hydrogen bond was shown as green, the halogen bond was shown as cycan.

As shown in Figure 4, both pyrimidone fragments of **23e** and **27g** stretched into the interior part of the binding groove of GSK-3*β*, and tacrine units adhered to the exterior section of the active pocket (Fig. 4A/B). The binding positions of compounds with GSK-3*β* still had notable differences in molecular orientation mainly because of the pyrimidone moiety bearing a fluorine-substituted pyridine group, generating optimal steric configurations for each other. Hybrid **23e** formed a hydrogen bond (2.0 Å) with interior residue Val-135 and a π-cation interaction (3.0 Å) with exterior residue Lys-183 (Fig. 4C). Hybrid **27g** had two hydrogen bonds with Val-135 (2.6 Å) and Lys-85 (2.7 Å) and a π-cation interaction (4.5 Å) with residue Arg-141 located on the opposite side of the peripheral groove (Fig. 4D). Even though the fluorine group did not participate in the formation of secondary bonds directly, its introduction had a favorable effect on forming more hydrogen bonds with GSK-3*β* by adjusting the steric configuration of **27g** to a more suitable binding position. Similarly, the docking results of GSK-3*β* were consistent with the SARs of hybrids.

To investigate whether the linker length of **27g** (hepta-methylene) was extended to octa- or nona-methylene, the relevant compounds were docked with AChE and GSK-3*β*, respectively. As shown in Figure S3a-f, octa- or nona-methylene-linked hybrids formed fewer secondary bonds with either AChE or GSK-3*β* than **27g**, which suggested that a linear chain of seven carbons was more suitable for the balance of dual-target potencies.

Hence, compound **27g** could fit the binding pockets of AChE and GSK-3*β* and exhibited good affinity with the interactions of several secondary bonds through the cooperation of the tacrine unit, alkylamine linker, and pyrimidone moiety, making it an excellent dual AChE/GSK-3*β* inhibitor. The introduction of a chlorine group on the tacrine unit and a fluorine group on the pyrimidione moiety is a feasible modification strategy, as demonstrated by SARs and molecular docking.

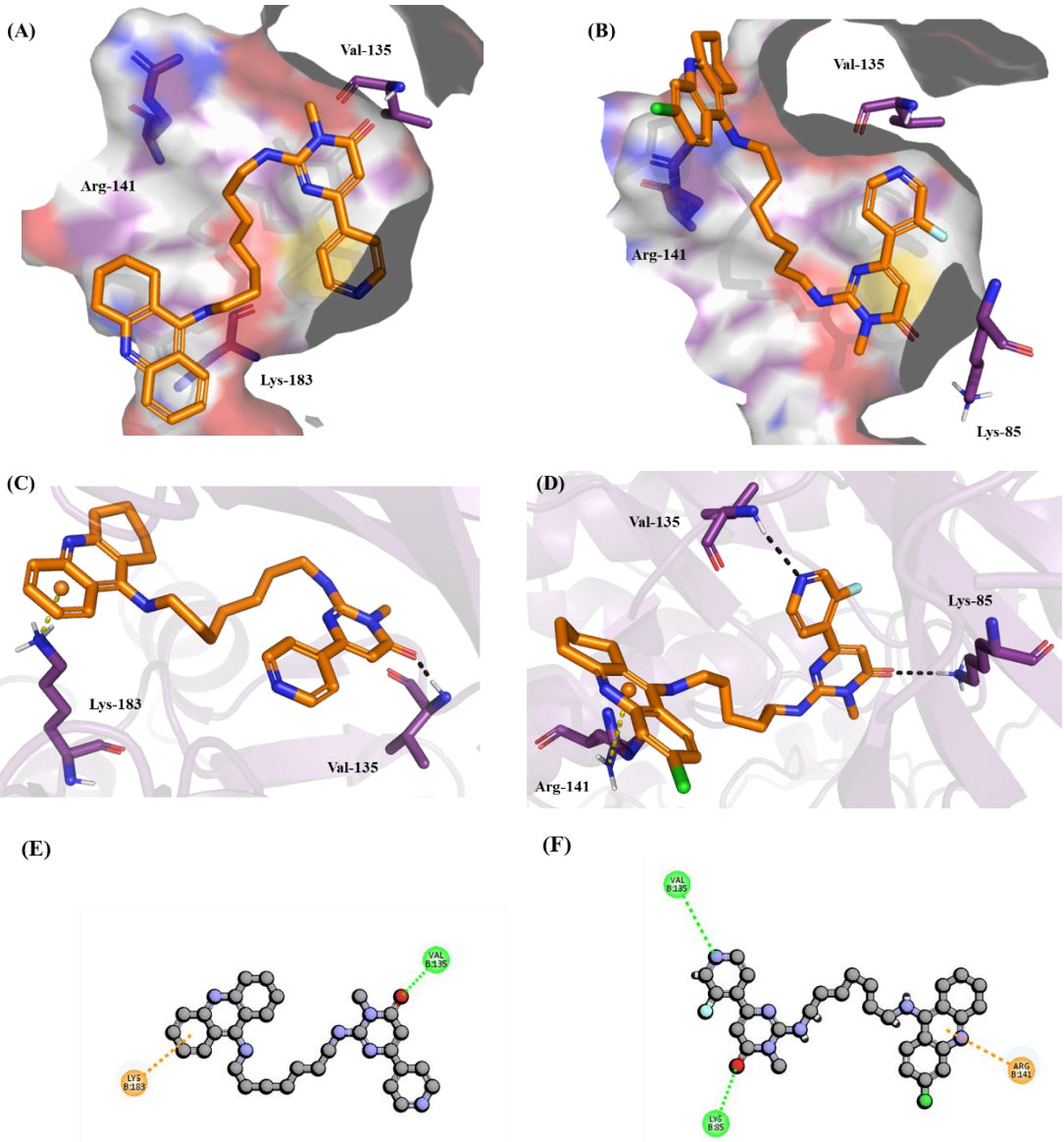

Figure 4. Proposed binding models of **23e** (A/C) or **27g** (B/D) with GSK-3*β* (PDB code: 3F88). For secondary bonds, hydrogen bonds were shown as black dotted lines, π-cation interactions were shown as yellow dotted lines. (A) The relative position of compound **23e** (shown in brown) in the active pocket of GSK-3*β*. (B) The relative position of **27g** (shown in brown) in the active pocket of GSK-3*β*. (C) Interactions between **23e** (shown in brown) and amino acid residue of GSK-3*β*. (D) Interactions between **27g** (shown in brown) and amino acid residue of GSK-3*β*. (E) The 2D binding mode of compound **23e** with GSK-3*β*, the hydrogen bond was shown as green, the π-cation bond was shown as orange. (F) The 2D binding mode of compound **27g** with GSK-3*β*, the hydrogen bond was shown as green, the π-cation bond was shown as orange.

Inhibition against the tau protein phosphorylation

The ability of **27g** to regulate the tau protein signaling pathway was further investigated using SH-SY5Y neuronal cultures[45] derived from the human neuroblastoma cell line SH-SY5Y under continuous treatment with retinoic acid (RA) (for more details, see the Experimental Section).

The exposure of SH-SY5Y neurons to glyceraldehyde (GA), an inhibitor of glycolysis, results in glycolytic inhibition, cell apoptosis, and an increase in tau protein phosphorylation.[46] For GA-induced SH-SY5Y-derived neurons, the p-Tau levels on serine-199 (S199) and serine-396 (S396) sites, the primary phosphorylation sites of tau protein catalyzed by GSK-3β,[47] were measured to evaluate the inhibitory capacity of **27g** for tau protein phosphorylation, with tideglusib (**10**) as a positive control, which is a typical selective GSK-3β inhibitor (Fig. 1C).[48]

As shown in Figure 5, dramatically induced tau protein phosphorylation in SH-SY5Y neurons compared with the blank neuronal group. In contrast with the model group, compound **27g** presented a significant reduction in p-Tau levels at both the S199 and S396 sites in a dose-dependent manner. In detail, **27g** exerted an obvious inhibitory effect on the p-Tau level at a relatively low concentration (10 nM) and a favorable ameliorative effect close to that of the blank group at superior concentrations (0.5 μM, 5 μM). The results of SH-SY5Y-derived neurons treated with tideglusib confirmed again that the key enzyme GSK-3β was responsible for tau protein phosphorylation in the GA-induced neuronal model. Therefore, compound **27g** with potent GSK-3β inhibition was proven to have the ability to regulate the tau protein pathway in SH-SY5Y-derived neurons.

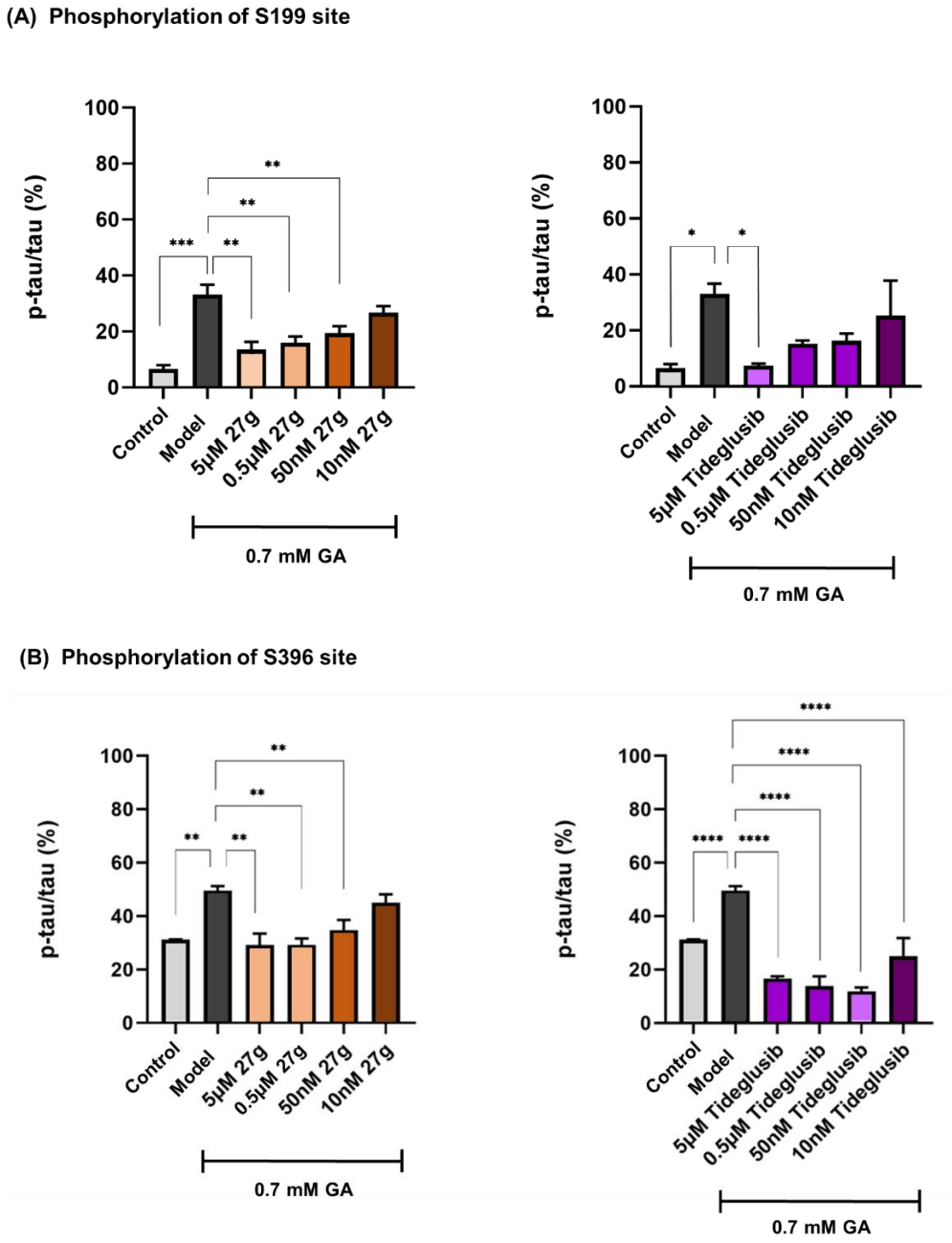

Figure 5. Quantification of phosphorylation ratio about p-Tau/total tau of GA treated SH-SY5Y differentiated neurons after **27g** or tideglusib treatment at different concentrations. Kuskar-Wallis test followed by Dunn's post-hoc was used to compare the differences between different groups. Data are expressed as mean ± SEM (at least n=3 independent experiments were performed; *$p < 0.05$, **$p < 0.01$, ***$p < 0.001$, ****$p < 0.0001$. (A) Phosphorylation results about p-Tau/total tau on S199 site of tau protein. (B) Phosphorylation results about p-Tau/total tau on S396 site of tau protein.

Alleviation against GA-induced cytotoxicity in differentiated SH-SY5Y cells

Neuronal damage caused by NFTs and SP is one of the major issues in AD progression, aggravating the disease condition and threatening the life of patients.[49] As neurons cannot actively replicate,[50] preventing neuronal loss is a crucial goal for any potential therapy. To assess whether compound **27g** was able to protect neuronal cells from cytotoxic GA, cell viability experiments were conducted using SH-SY5Y-derived neurons.

As depicted in Figure 6, incubation of neurons with 0.7 mM GA caused serious toxicity.[46] In contrast with the model group, the presence of compound **27g** or the positive control tideglusib at different concentrations (0.5 μM, 5 μM) resulted in a significant increase in cell viability, indicating that these two compounds had neuroprotection towards SH-SY5Y neurons. The holistic results suggested the central role of tau protein phosphorylation, which played a pivotal function in GA-induced cytotoxicity, and **27g** could reverse the detrimental effect of GA by inhibiting GSK-3β and improving the tau protein signaling pathway.

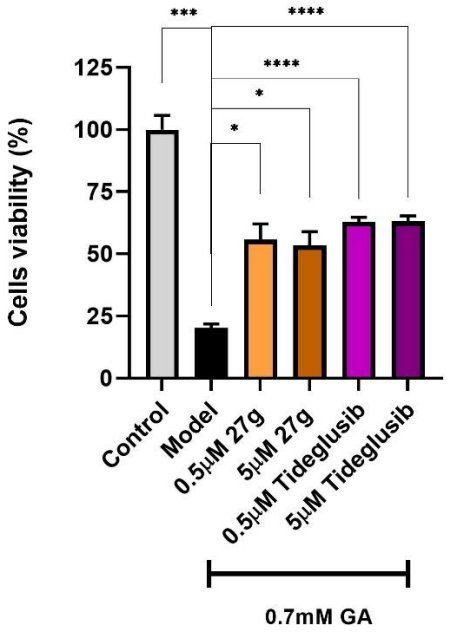

Figure 6. Cell viability of SH-SY5Y differentiated neurons following the treatment of GA, compound **27g** or tideglusib at different concentrations. Ordinary one-way ANOVA followed by Tukey's post-hoc test was used to compare differences between different groups. Data are presented as the mean ± SEM (at least n = 9 independent experiments were performed; *$p < 0.05$, ***$p < 0.001$, ****$p < 0.0001$).

Alleviation against GA-induced morphological damage in differentiated SH-SY5Y cells

Cytoskeletal architecture plays a crucial role in maintaining neural morphology and synaptic plasticity,[51] forming a correct network between multiple neurons. During the progression of AD, this architecture is jeopardized due to the formation of NFTs, which leads to neuronal destruction and apoptosis. Incubation of SH-SY5Y cells with RA results in typical neural networking, with a significant increase in axon length compared to SH-SY5Y cells.[45] Treatment with 0.7 mM GA results in a dramatic increase in tau protein phosphorylation and, in turn, results in neurite dystrophy and loss of network between SH-SY5Y-derived neurons.

Next, morphology studies were conducted to determine whether compound **27g** can maintain the axon length of neurons in the presence of GA. As shown in Figure 7A, compound **27g** (0.5 μM, 5 μM) significantly prevented neurite shortening in a dose-dependent manner and exhibited more potent improvement effects than tideglusib at the same concentrations. Confocal images of the corresponding neuronal groups are displayed in Figure 7B to show the destruction of GA (Fig. 7B3) and the reversible ability of **27g** (Fig. 7B4/5) and tideglusib (Fig. 7B6/7) in a more visual way. These similar results with **27g** and tideglusib suggested that the adverse effect of axon length induced by GA was implicated in the disorder of the tau protein signaling pathway, indicating once again that compound **27g** could exert neuroprotection against SH-SY5Y-derived neurons as a GSK-3β inhibitor.

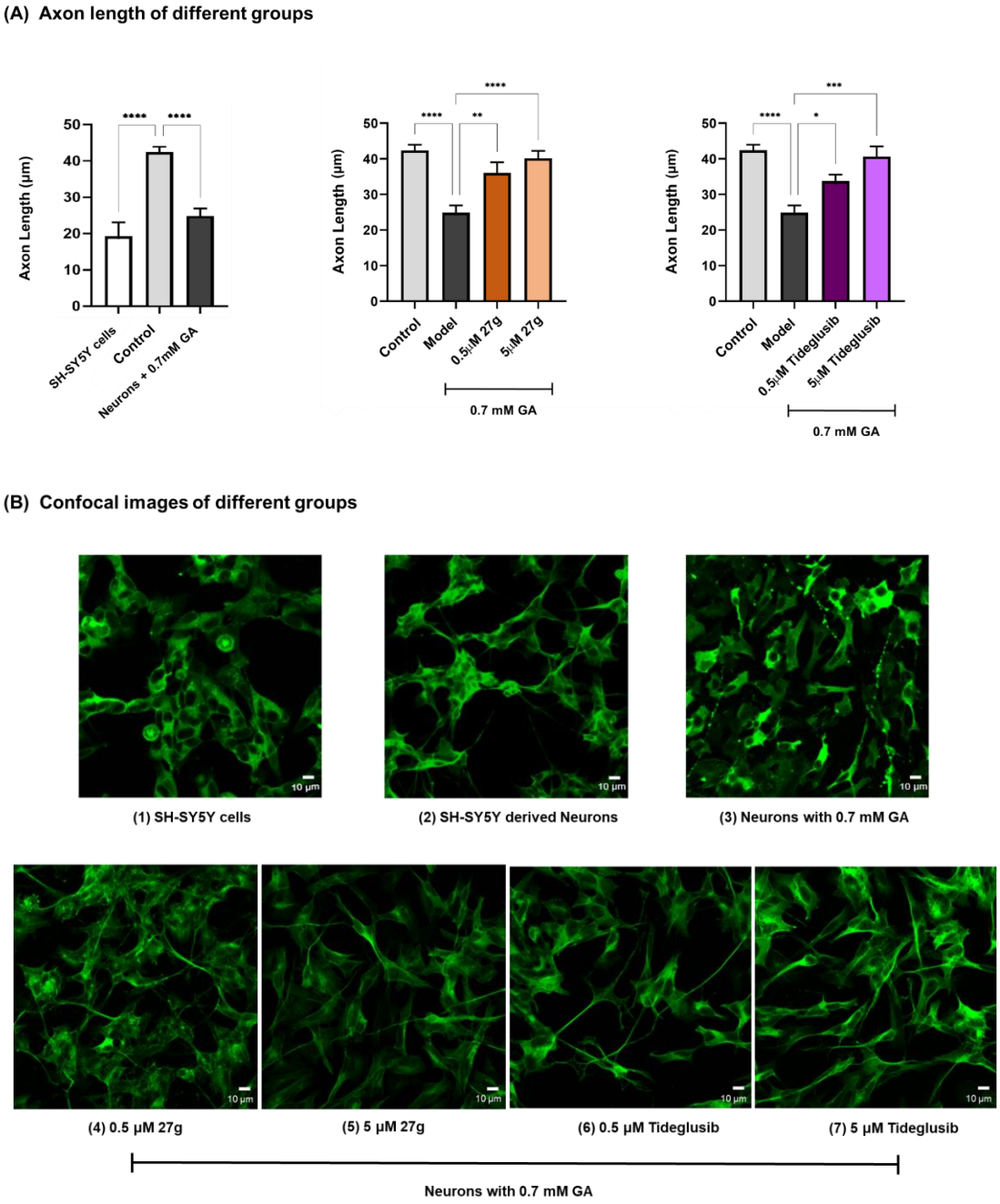

Figure 7. Morphology studies of SH-SY5Y derived neurons. Ordinary one-way ANOVA followed by Tukey's post-hoc test was used to compare differences between different groups. Data are presented as mean ± SEM (at least n = 3 independent experiments were performed; *$p < 0.05$, **$p < 0.01$, ***$p < 0.001$, ****$p < 0.0001$). (A) Axon length quantification of 0.7 mM GA treated SH-SY5Y differentiated neurons after **27g** or tideglusib treatment at different concentrations. (B) Confocal images of 0.7 mM GA treated SH-SY5Y differentiated neurons after **27g** or tideglusib treatment at different concentrations.

Kinase selectivity profiling of 27g

To further investigate kinase selectivity, a panel of 205 kinase selectivity profiles of compound **27g** was measured at a concentration of 1000 nM. As shown in Figure 8, the results indicated that compound **27g** displayed weak inhibitory activities against almost all of the tested kinases except GSK3*α*. This result suggested that compound **27g** was a pan-GSK-3 inhibitor and possessed good kinase selectivity profiles.

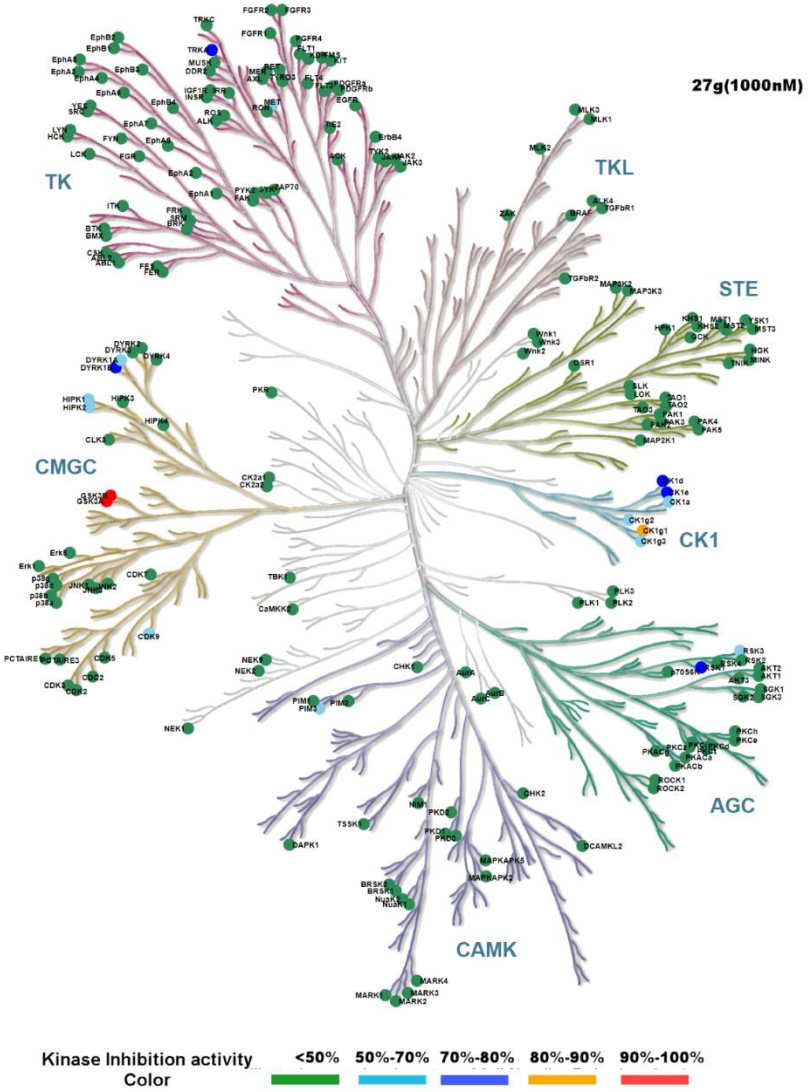

Figure 8. TREEspot maps for **27g** against 205 kinases (ICE Bioscience Inc.). A concentration of 1000 nM was used for the measurements, and the affinity was defined as a percent of the DMSO control (% control).

Pharmacokinetic properties investigation

The pharmacokinetic profiles of a promising compound can provide important information with regard to its absorption, distribution, metabolism, and excretion (ADME) properties, which become

crucial references to predict its manifestation in the human body.[52] Therefore, an *in vivo* pharmacokinetic investigation of compound **27g** in ICR mice was conducted to validate its ADME characteristics, and the results are shown in Table 3 and Table S4-6.

Obviously, the intravenous (i.v.) administration (5 mg/kg) showed better performance for the use of **27g** than i.p. injection (15 mg/kg). I.v. injection had a shorter t_{max} (0.033 h) and higher C_{max} (2807 ng/mL), similar values for the area under curve (AUC) and apparent volume of distribution (V_d), and a longer half-life ($t_{1/2}$ = 3.65 h), longer mean residence time (MRT = 3.05 h), and smaller clearance rate (CL = 3.08 L/h/kg) in terms of excretion when compared with i.p. administration. Notably, the data derived from i.p. injection of **27g** were still valid and positive under comprehensive estimation. Moreover, the pharmacokinetic data of i.p. administration were acceptable for moving compound **27g** to *in vivo* study as a tool to validate the potential of the series with a half-life of 1.15 h and bioavailability (*F*) of 35.3%.

The eligible performance of compound **27g** demonstrated its potential as a lead compound and suggested that further modification based on its ADME properties is needed to acquire more extensive application approaches and more potent adjustments towards the disease network of AD.

Table 3. Pharmacokinetic Parameters of **27g** after Its Administration[a]

Administration	$t_{1/2}$ (h)	t_{max} (h)	C_{max} (ng/mL)	AUC_{last} (h*ng/mL)	V_d (L/kg)	$CL_{\_F\_obs}$ (L/h/kg)	MRT_{last} (h)	F (%)
I.V. 5 mg/kg	3.65 ± 1.05	0.033 ± 0.000	2807 ± 1113	1564 ± 93	16.42 ± 5.94	3.08 ± 0.24	3.05 ± 2.09	-
I.P. 15 mg/kg	1.15 ± 1.18	0.139 ± 0.096	1868 ± 392	1658 ± 222	14.14 ± 13.14	9.12 ± 1.30	0.78 ± 0.33	35.3

[a]Values are expressed as the mean ± SD (n = 3).

Blood-brain barrier permeability assay

AD pathology is fundamentally implicated in disordered enzymes and morbid regions inside the brain, and drugs aiming to regulate AD-related targets need the ability to penetrate the blood-brain

barrier (BBB) and form gradual enrichment at the interior of the brain after their administration.[53] Thus, an *in vivo* assay of **27g** in ICR mice was performed to evaluate its permeability to the BBB and its qualification as a truly available AChE/GSK-3 inhibitor.

From the results presented in Table 4 and Table S7, hybrid **27g** was clearly detected in both the plasma and brain after intraperitoneal (i.p.) administration at the dosage of 15 mg/kg. Along with the change of time (0.5-4 h), the concentration of **27g** in plasma decreased in a relatively rapid way (866.5-3.5 ng/mL), while the downtrend of **27g** in the brain was torpid, and there was even an increase in the period of 1-2 h (11.2-12.2 ng/g). The value of blood/plasma steadily increased from the initial 0.028 to 1.924, and the amount of **27g** in the brain surpassed its quantities in plasma after four hours of metabolism. Data from this assay demonstrated that **27g** could partially penetrate the brain and accumulate in this tissue, being removed slower than that from the plasma. Therefore, further modification is still needed to acquire molecules with better BBB permeability.

Table 4. The Concentration of **27g** in Plasma and Brain after Its i.p. Administration (15 mg/kg) [a]

T (h)	Concentration of **27g**		Ratio of Brain/Plasma
	Plasma (ng/mL)	Brain (ng/g)	
0.5	866.5 ±205.8	23.63 ±4.78	**0.028** ±0.007
1	76.75 ±14.41	11.13 ±1.18	**0.148** ±0.025
2	26.75 ±12.74	12.23 ±2.06	**0.522** ±0.189
4	3.469 ±1.433	5.994 ±1.043	**1.924** ±0.759

[a]Values are expressed as the mean ±SD (n = 4).

Behavioral studies in AD-related mice model

The paramount goal of outstanding anti-AD drugs, such as donepezil (**1**) and memantine (**6**), is to strongly improve the cognition and memory conditions of patients. The most common approach to investigate the ability of promising anti-AD agents to improve the behavior of mice is the classical Morris water maze (MWM) test in preclinical research.[54] Thus, scopolamine-induced cognition-impaired ICR mice were adopted to evaluate the overall amelioration effects of compounds **23e** and **27g**, two representative hybrids in our work, using a modified MWM test.[55]

Forty female ICR adult mice (8-10 weeks) were randomly distributed into five groups (n = 8 for

each group): blank control, model (scopolamine), tacrine, **23e**, and **27g**. The blank solvent for the blank control group was phosphate-buffered saline (PBS) with 10% dimethyl sulfoxide (DMSO) and 20% (2-hydroxypropyl)-β-cyclodextrin, and the dosages of agents for other groups were unified as 15 mg/kg in the blank solvent. The entire experimental period was 25 d, and the blank control group was treated with blank solvent each day. Other groups were treated with scopolamine (i.p.) for the initial 10 consecutive days[56]. Tacrine, **23e**, and **27g** for the respective group were i.p. injected into the ICR mice 30 min after the administration of scopolamine in the following 15 consecutive days. Days 21-24 were the training period for mice in all groups to incrementally learn the location of the fixed and hidden platform in the fourth quadrant of the maze, and a spatial probe trial was conducted and recorded on days 23-25. The mean values presented in Figure 10 and Table S7 show the latencies and distances for mice to reach the first escape entry on days 23-24. An additional test item on day 25 was used to assess the memory retention of mice by removing the hidden platform from the maze, and entry times for mice arriving at the virtual platform were recorded, as shown in Figure 9 and Table S8.

Excellent behavior performance for mice required faster escape latency (Fig. 9A), shorter searching distance (Fig. 9B), and more arrival times (Fig. 9C). The cognitive competence of the blank control group exhibited the optimal performance (9.40 s, 2.07 m, n = 6.79, respectively), and the model group treated with scopolamine had relatively poor results (23.81 s, 5.00 m, n = 3.63, respectively), indicating that the scopolamine-induced cognition-impaired animal model worked well. As the positive control, tacrine efficiently improved the overall memory and cognition of mice (10.76 s, 2.42 m, n = 6.56, respectively). Moreover, sample groups treated with **23e** and **27g** displayed remarkable behavior enhancement based on the data of the model group, and **27g** (11.86 s, 2.46 m, n = 6.44, respectively) showed slightly more potent amelioration of cognition and memory than **23e** (14.08 s, 2.50 m, n = 6.10, respectively), indicating that the *in vitro* advantage of **27g** in AChE/GSK-3β inhibition could reflect an authentic *in vivo* AD-related animal model. Given the same dosage of agents (15 mg/kg), the smaller molecular weight of tacrine (M.W. = 237.72) led to its higher concentration, while mice treated with compound **27g** (M.W. = 549.09) still exhibited similar performance on the MWM test, approaching the therapeutic effects of tacrine. Furthermore, the i.p. injection of **23e** and **27g** caused no abnormal events (emesis or diarrhea) or swimming motility impairment in mice throughout the entire experimental period, which demonstrated their

safety for long-term administration at the dosage of 15 mg/kg for each day.

Taken together, the overall behavioral performance in the MWM assay observed in the **23e** and **27g** groups supports their capacities to significantly ameliorate the impairment caused by scopolamine, possessing an analogous effect to tacrine at the same administered dosage.

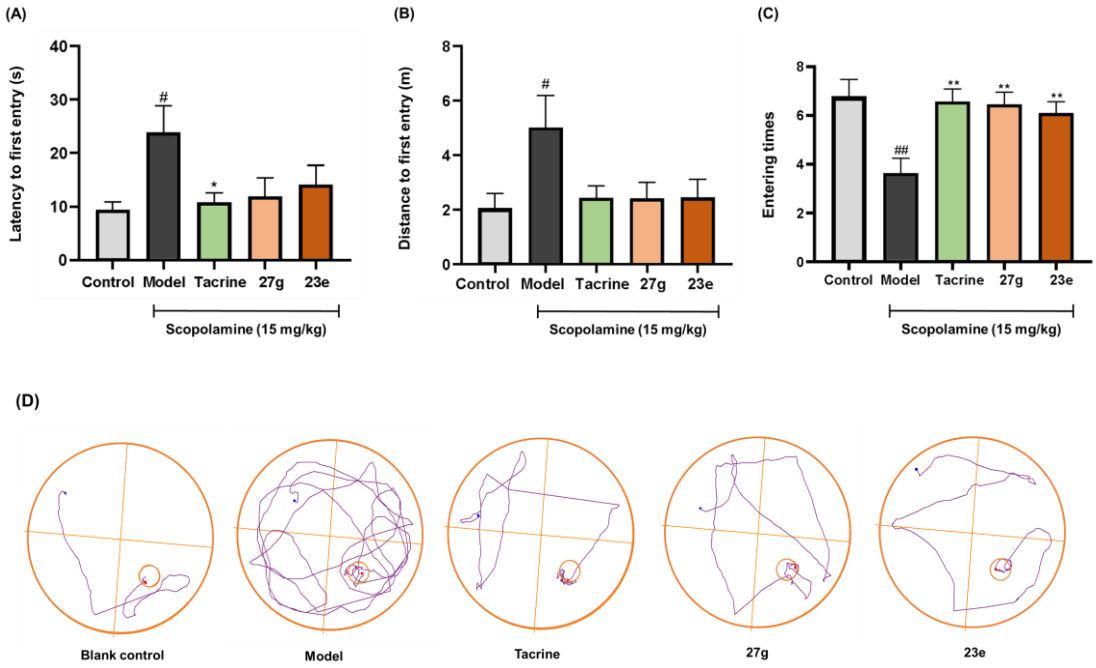

Figure 9. Effects of i.p. administration of **27g** (15 mg/kg), **23e** (15 mg/kg), and tacrine (**4**, 15 mg/kg) on scopolamine-induced cognitive impairment in ICR mice evaluated by the Morris water maze test. Data are presented as the mean ± SEM (n = 8; $^{\#}p \leq 0.05$, $^{\#\#}p \leq 0.01$ *vs* blank control group; $^{*}p \leq 0.05$, $^{**}p \leq 0.01$ *vs* scopolamine group). (A) The latency for mice to reach the first escape entry. (B) The distance for mice to reach the first escape entry. (C) The number of entering times for mice to the virtual platform (the original platform location). (D) The representative tracks of mice in MWM during the spatial probe trial period.

CONCLUSIONS

In summary, it is not easy to find the potentially curable treatment of AD, whereas regulating cholinergic and tau protein signaling pathways by a single molecule in AD-related studies will play an essential role in achieving a better treatment effect of AD. Based on the multi-target strategy, a series of dual AChE/GSK-3 inhibitors were innovatively designed and easily synthesized by using tacrine (**4**) and pyrimidone structures as parent building blocks. Optimization has resulted in fifty tacrine-pyrimidone hybrids, which exhibited integrated and detailed SARs with IC_{50} levels

enhanced from the micromole to nanomole level against AChE and GSK-3β *in vitro*. Furthermore, several promising compounds were discovered to possess excellent characteristics, of which compound **27b** displayed the best AChE inhibition, compound **27j** showed the most potent GSK-3β inhibition, and compound **27g** simultaneously possessed favorable inhibitory potency and inhibitory equilibrium against two targets, becoming the optimal hybrid among the series of new compounds. Furthermore, molecular docking studies rationally predicted the binding patterns between hybrids (**23e** and **27g**) and enzymes, and clearly demonstrated the binding difference influenced by key substituted groups, which is in agreement with the actual assay results of compounds against dual targets.

The GA-induced phosphorylation of tau protein on S199 and S396 sites could be dose-dependently suppressed with treatment by **27g** in SY-SY5Y derived neurons, indicating the beneficial regulation of **27g** on the tau protein signaling pathway as a GSK-3β inhibitor. Thus, evidence has shown that the inhibitory activities of compound **27g** at the enzyme level could present macroscopic improvement at the nervous tissue and animal levels, suggesting that **27g** has the potential to synergistically adjust the two pathways, which is an outstanding therapeutic option for the prospective treatment of AD. For adverse effects induced by GA, the evident neuroprotective effect of **27g** on SH-SY5Y-derived neurons was verified through cell viability assays and morphology surveys. Kinase selectivity profiling study showed that compound **27g** is a pan-GSK-3 inhibitor and possessed good kinase selectivity profiles.

Furthermore, the capacity of **27g** to successfully permeate the BBB and locate in the brain and the eligible pharmacokinetic parameters of **27g** were confirmed by *in vivo* assays in mice with the auxiliary detection of UPLC-MS/MS. In the preliminary hepatotoxicity study, oral administration of compound **27g** to mice showed only weak hepatotoxity, which would not disrupt the physiological function of the liver (Tables S9). In particular, the ability of **27g** to improve cholinergic deficits and disorder of the tau protein pathway was investigated. Scopolamine-induced ICR mice treated with **27g** (15 mg/kg/day) showed significant amelioration of memory performance and spatial behavior in the MWM test, indicating that the cholinergic signaling pathway could be enhanced by **27g** as an AChE inhibitor.

In conclusion, this work validates the multitarget anti-AD strategy by fusing tacrine and pyrimidone for the first time, identifying a series of novel hybrids with excellent dual AChE/GSK-

3 inhibition. All of the pharmacological results highlight that the most promising compound, **27g**, possesses multiple anti-AD profiles with benign safety and drug-like properties. And therefore, **27g** can be considered a potential prototype to be further developed for the better treatment of AD.

EXPERIMENTAL SECTION

Chemistry

General methods. Unless otherwise stated, all reagents were purchased from Energy Chemical (China) or Bidepharm (China). AR-A014418 was purchased from Selleck (Catalog No.S7435). All commercially available reagents (reagent grade) were used without further purification. THF was dried through routine protocols using metal sodium. Flash column chromatography was performed on 200-300 mesh silica gel (Qingdao Haiyang Chemical, China). Reactions were monitored by thin-layer chromatography (TLC) on 0.25 mm silica gel GF_{254} plates and visualized under UV light (λ = 254 nm). ^{1}H NMR and ^{13}C NMR spectra were recorded by a Bruker AV-300 spectrometer (Bruker Company, Germany) in the indicated solvents ($CDCl_3$, CD_3OD, or DMSO-d_6) and referenced to internal standard tetramethylsilane. Chemical shifts were reported in ppm (δ) values and the coupling constants (J) in Hz. Proton coupling patterns were described as singlet (s), broad singlet (brs), doublet (d), doublet of doublets (dd), triplet (t), quartet (q), and multiplet (m). The high-resolution mass spectrometry (HRMS) was measured on a Finnigan MAT 95 spectrometer (Finnigan, Germany). The analytical samples of target compounds possessed satisfactory purity (> 95%), according to their respective NMR spectra, high-performance liquid chromatography (HPLC) and HRMS measurements (for more details, see the Supporting Information).

For key intermediates shown in schemes 1-2, compounds **14a**, **14b**, and **14c** were successfully synthesized according to Uehara's work (compound **28**),[37] and Fukunaga's work (compound **6**,[38] compound **26**[40]), respectively. And analogues **18a-m**, **19a-e**, **24a-e**, and **25a-e** which are different tacrine derivatives bearing respective alkylamine, were smoothly synthesized according to Sun's work using the similar method.[30] The synthesis of representative intermediates was described in Supporting Information.

General procedures for the synthesis of target compounds **21a-m**, **22a-j**, **23a-e**, **26a-k**, and **27a-k**. To a solution of key intermediate **14** (0.45 mmol, 1 eq) in THF (8 mL) was added specific tacrine derivative (0.45 mmol, 1 eq) from **18**, **19**, **24** or **25**. Subsequently, base K_2CO_3 (1.35 mmol, 3 eq)

was added to the solution, and the reaction mixture was stirred overnight at 66 °C. Then, the mixture was extracted with EtOAc (3 × 20 mL) after the addition of water, and the combined organic layers were washed with saturated brine and dried over anhydrous Na_2SO_4. Removal of the solvent in vacuo produced a residue which was purified by column chromatography, using gradient eluent from petroleum ether/EtOAc (1:3) to dichloromethane/methanol (10:1), to afford corresponding target compound in good yield.

3-Methyl-6-(pyridin-4-yl)-2-((2-((1,2,3,4-tetrahydroacridin-9-yl)amino)ethyl)amino)pyrimidin-4(3*H*)-one (**21a**). White solid, 62% yield: Rf = 0.4 (10% methanol in dichloromethane). ^{1}H NMR (300 MHz, CD_3OD) δ 8.54 (d, *J* = 5.7 Hz, 2H), 8.38 (d, *J* = 8.7 Hz, 1H), 7.75 (dd, *J* = 13.0, 6.5 Hz, 3H), 7.58 (d, *J* = 8.5 Hz, 1H), 7.43 (t, *J* = 7.5 Hz, 1H), 6.29 (s, 1H), 4.33 (s, 2H), 4.06 (s, 2H), 3.31 (s, 3H), 2.78 (d, *J* = 5.9 Hz, 2H), 2.44 (s, 2H), 1.84 - 1.59 (m, 4H). ^{13}C NMR (75 MHz, CD_3OD) δ 167.0, 161.3, 160.8, 159.0, 154.4, 154.0, 154.0, 148.6, 142.1, 136.6, 129.3, 129.0, 124.8, 124.8, 123.4, 120.2, 115.9, 102.3, 45.5, 32.2, 31.4, 31.4, 28.4, 25.7, 24.5. HRMS (ESI) *m/z*: calcd for $C_{25}H_{27}N_6O$ $[M+H]^+$ 427.2241, found 427.2236.

2-((2-((6-Methoxy-1,2,3,4-tetrahydroacridin-9-yl)amino)ethyl)amino)-3-methyl-6-(pyridin-4-yl)pyrimidin-4(3*H*)-one (**21b**). White solid, 53% yield: Rf = 0.5 (9% methanol in dichloromethane). ^{1}H NMR (400 MHz, CD_3OD) δ 8.56 (dd, *J* = 4.6, 1.6 Hz, 2H), 8.29 (d, *J* = 9.5 Hz, 1H), 7.77 (dd, *J* = 4.6, 1.6 Hz, 2H), 7.01 (dd, *J* = 9.5, 2.6 Hz, 1H), 6.88 (d, *J* = 2.6 Hz, 1H), 6.35 (s, 1H), 4.36 - 4.19 (m, 2H), 4.10 - 4.02 (m, 2H), 3.96 (s, 3H), 3.32 (s, 3H), 2.76 (t, *J* = 6.1 Hz, 2H), 2.37 (t, *J* = 5.8 Hz, 2H), 1.81 - 1.61 (m, 4H). ^{13}C NMR (75 MHz, CD_3OD) δ 167.8, 166.7, 161.8, 160.2, 159.2, 153.5, 153.5, 152.9, 149.2, 144.8, 130.7, 125.1, 125.1, 120.8, 114.5, 114.1, 103.1, 102.5, 59.6, 45.0, 31.8, 31.6, 31.6, 27.6, 25.4, 24.4. HRMS (ESI) *m/z*: calcd for $C_{26}H_{29}N_6O_2$ $[M+H]^+$ 457.2347, found 457.2342.

2-((2-((6-Chloro-1,2,3,4-tetrahydroacridin-9-yl)amino)ethyl)amino)-3-methyl-6-(pyridin-4-yl)pyrimidin-4(3*H*)-one (**21c**). White solid, 58% yield: Rf = 0.5 (10% methanol in dichloromethane). ^{1}H NMR (400 MHz, CD_3OD) δ 8.57 (dd, *J* = 4.6, 1.6 Hz, 2H), 8.36 (d, *J* = 9.2 Hz, 1H), 7.76 (dd, *J* = 4.6, 1.6 Hz, 2H), 7.56 (t, *J* = 4.3 Hz, 1H), 7.36 (dd, *J* = 9.2, 2.1 Hz, 1H), 6.35 (s, 1H), 4.36 - 4.26 (m, 2H), 4.10 - 4.02 (m, 2H), 3.66 (d, *J* = 3.2 Hz, 1H), 3.33 (s, 3H), 2.82 (t, *J* = 6.2 Hz, 2H), 2.44 (s, 2H), 1.84 - 1.65 (m, 4H). ^{13}C NMR (75 MHz, CD_3OD) δ 167.8, 161.8, 160.1, 159.2, 154.8, 153.5, 153.5, 149.2, 143.2, 142.7, 130.7, 129.7, 125.1, 125.1, 122.4, 118.2, 116.1, 103.3, 45.0, 32.2, 31.7,

31.7, 28.0, 25.3, 24.3. HRMS (ESI) *m/z*: calcd for $C_{25}H_{26}ClN_6O$ $[M+H]^+$ 461.1852, found 461.1850.

2-((2-((7-Methoxy-1,2,3,4-tetrahydroacridin-9-yl)amino)ethyl)amino)-3-methyl-6-(pyridin-4-yl)pyrimidin-4(3*H*)-one (**21d**). White solid, 56% yield： Rf = 0.5 (10% methanol in dichloromethane). ^{1}H NMR (400 MHz, CD_3OD) δ 8.57 (dd, *J* = 4.6, 1.6 Hz, 2H), 7.71 (dd, *J* = 4.6, 1.6 Hz, 2H), 7.48 (dd, *J* = 7.4, 5.9 Hz, 2H), 7.37 (dd, *J* = 9.2, 2.5 Hz, 1H), 6.21 (s, 1H), 4.33 - 4.23 (m, 2H), 4.05 - 3.95 (m, 2H), 3.80 (s, 3H), 3.27 (s, 3H), 2.82 (t, *J* = 6.2 Hz, 2H), 2.66 (t, *J* = 5.8 Hz, 2H), 1.89 - 1.71 (m, 4H). ^{13}C NMR (75 MHz, CD_3OD) δ 167.8, 161.5, 161.1, 160.0, 158.7, 153.3, 153.3, 152.9, 149.1, 136.9, 127.9, 125.0, 125.0, 124.5, 121.9, 115.9, 107.5, 102.5, 59.8, 45.6, 32.0, 31.5, 31.5, 28.8, 25.7, 24.4. HRMS (ESI) *m/z*: calcd for $C_{26}H_{29}N_6O_2$ $[M+H]^+$ 457.2347, found 457.2343.

2-((2-((6-Fluoro-1,2,3,4-tetrahydroacridin-9-yl)amino)ethyl)amino)-3-methyl-6-(pyridin-4-yl)pyrimidin-4(3*H*)-one (**21e**). White solid, 59% yield：Rf = 0.4 (9% methanol in dichloromethane). ^{1}H NMR (400 MHz, CD_3OD) δ 8.58 (dd, *J* = 4.6, 1.6 Hz, 2H), 8.49 (dd, *J* = 8.8, 5.4 Hz, 1H), 7.79 (dd, *J* = 4.6, 1.6 Hz, 2H), 7.24 (dd, *J* = 14.4, 5.6 Hz, 2H), 6.37 (s, 1H), 4.38 - 4.27 (m, 2H), 4.16 - 4.03 (m, 2H), 3.35 (s, 3H), 2.80 (t, *J* = 6.2 Hz, 2H), 2.41 (s, 2H), 1.73 (m, 3H). ^{13}C NMR (75 MHz, CD_3OD) δ 170.0, 167.8, 166.6, 161.9, 160.6, 159.2, 154.4, 153.5, 153.5, 149.3, 132.4, 125.1, 125.1, 118.7, 116.7, 115.5, 108.0, 103.1, 45.0, 31.9, 31.6, 31.6, 27.9, 25.3, 24.3. HRMS (ESI) *m/z*: calcd for $C_{25}H_{26}FN_6O$ $[M+H]^+$ 445.2147, found 445.2146.

2-((2-((7-Fluoro-1,2,3,4-tetrahydroacridin-9-yl)amino)ethyl)amino)-3-methyl-6-(pyridin-4-yl)pyrimidin-4(3*H*)-one (**21f**). White solid, 60% yield：Rf = 0.4 (9% methanol in dichloromethane). ^{1}H NMR (400 MHz, CD_3OD) δ 8.58 (dd, *J* = 4.6, 1.6 Hz, 2H), 8.04 (dd, *J* = 10.6, 2.3 Hz, 1H), 7.77 (dd, *J* = 4.6, 1.6 Hz, 2H), 7.67 - 7.56 (m, 2H), 6.31 (s, 1H), 4.34 - 4.22 (m, 2H), 4.11 - 3.99 (m, 2H), 3.30 (s, 3H), 2.84 (t, *J* = 6.3 Hz, 2H), 2.55 (t, *J* = 5.7 Hz, 2H), 1.85 - 1.67 (m, 4H). ^{13}C NMR (75 MHz, CD_3OD) δ 167.8, 164.7, 161.7, 161.4, 158.9, 154.7, 153.3, 153.3, 149.1, 139.1, 126.4, 125.9, 125.8, 125.0, 125.0, 121.0, 116.2, 102.6, 45.3, 32.1, 31.2, 31.2, 28.4, 25.4, 24.3. HRMS (ESI) *m/z*: calcd for $C_{25}H_{26}FN_6O$ $[M+H]^+$ 445.2147, found 445.2141.

2-((2-((6-Bromo-1,2,3,4-tetrahydroacridin-9-yl)amino)ethyl)amino)-3-methyl-6-(pyridin-4-yl)pyrimidin-4(3*H*)-one (**21g**). White solid, 61% yield：Rf = 0.5 (10% methanol in dichloromethane). ^{1}H NMR (400 MHz, CD_3OD) δ 8.58 (dd, *J* = 4.6, 1.6 Hz, 2H), 8.28 (d, *J* = 9.1 Hz, 1H), 7.76 (dd, *J* = 4.6, 1.6 Hz, 2H), 7.72 (d, *J* = 1.9 Hz, 1H), 7.48 (dd, *J* = 9.2, 1.9 Hz, 1H), 6.35 (s, 1H), 4.36 - 4.27

(m, 2H), 4.12 - 4.00 (m, 2H), 3.33 (s, 3H), 2.82 (t, *J* = 6.2 Hz, 2H), 2.44 (s, 2H), 1.76 (m, 4H). ^{13}C NMR (75 MHz, CD_3OD) Given the property of 300 MHz spectrometer and the low solubility of compound in deuterated solvents, the ^{13}C NMR spectrum of **21g** was not successfully acquired. However, the ^{1}H NMR spectrum and HRMS data of **21g** afforded here could be the valid evidence for the structure of **21g**. HRMS (ESI) *m/z*: calcd for $C_{25}H_{26}BrN_6O$ $[M+H]^+$ 505.1346, found 505.1349.

3-Methyl-2-((2-((6-methyl-1,2,3,4-tetrahydroacridin-9-yl)amino)ethyl)amino)-6-(pyridin-4-yl)pyrimidin-4(3*H*)-one (**21h**). White solid, 65% yield： Rf = 0.5 (10% methanol in dichloromethane). ^{1}H NMR (400 MHz, CD_3OD) δ 8.56 (dd, *J* = 4.7, 1.4 Hz, 2H), 8.27 (t, *J* = 8.9 Hz, 1H), 7.76 (dd, *J* = 4.7, 1.5 Hz, 2H), 7.34 (s, 1H), 7.25 (d, *J* = 8.9 Hz, 1H), 6.34 (s, 1H), 4.37 - 4.28 (m, 2H), 4.10 - 4.01 (m, 2H), 3.30 (s, 3H), 2.79 (t, *J* = 6.1 Hz, 2H), 2.51 (s, 3H), 2.43 (s, 2H), 1.83 - 1.65 (m, 4H). ^{13}C NMR (75 MHz, CD_3OD) δ 167.8, 161.8, 160.7, 159.0, 153.4, 153.3, 153.3, 149.1, 148.1, 142.4, 131.1, 128.7, 125.1, 125.1, 121.9, 117.9, 115.2, 102.6, 45.2, 31.8, 31.3, 31.3, 27.8, 25.4, 24.8, 24.3. HRMS (ESI) *m/z*: calcd for $C_{26}H_{29}N_6O$ $[M+H]^+$ 441.2397, found 441.2396.

3-Methyl-2-((2-((7-methyl-1,2,3,4-tetrahydroacridin-9-yl)amino)ethyl)amino)-6-(pyridin-4-yl)pyrimidin-4(3*H*)-one (**21i**). White solid, 63% yield：Rf = 0.5 (10% methanol in dichloromethane). ^{1}H NMR (400 MHz, CD_3OD) δ 8.58 (dd, *J* = 4.6, 1.6 Hz, 2H), 8.04 (s, 1H), 7.76 (dd, *J* = 4.6, 1.6 Hz, 2H), 7.58 (dd, *J* = 8.6, 1.3 Hz, 1H), 7.47 (d, *J* = 8.6 Hz, 1H), 6.26 (s, 1H), 4.37 - 4.27 (m, 2H), 4.08 - 3.97 (m, 2H), 3.28 (s, 3H), 2.81 (t, *J* = 6.2 Hz, 2H), 2.58 (s, 2H), 2.37 (s, 3H), 1.88 - 1.65 (m, 4H). ^{13}C NMR (75 MHz, CD_3OD) δ 167.7, 161.5, 160.4, 158.8, 153.3, 153.3, 149.0, 140.2, 139.6, 138.5, 127.2, 124.9, 124.9, 122.7, 120.2, 115.6, 102.7, 97.2, 45.2, 31.8, 31.5, 31.5, 28.2, 25.4, 25.0, 24.3. HRMS (ESI) *m/z*: calcd for $C_{26}H_{29}N_6O$ $[M+H]^+$ 441.2398, found 441.2396.

2-((2-((7-Chloro-1,2,3,4-tetrahydroacridin-9-yl)amino)ethyl)amino)-3-methyl-6-(pyridin-4-yl)pyrimidin-4(3*H*)-one (**21j**). White solid, 60% yield：Rf = 0.5 (10% methanol in dichloromethane). ^{1}H NMR (400 MHz, CD_3OD) δ 8.59 (dd, *J* = 4.6, 1.6 Hz, 2H), 8.28 (d, *J* = 1.8 Hz, 1H), 7.79 (dd, *J* = 4.6, 1.6 Hz, 2H), 7.70 (dd, *J* = 9.0, 2.0 Hz, 1H), 7.56 (d, *J* = 9.0 Hz, 1H), 6.31 (s, 1H), 4.35 - 4.22 (m, 2H), 4.09 - 3.97 (m, 2H), 3.30 (s, 3H), 2.85 (t, *J* = 6.3 Hz, 2H), 2.60 (s, 2H), 1.80 (m, 4H). ^{13}C NMR (75 MHz, CD_3OD) Given the property of 300 MHz spectrometer and the low solubility of compound in deuterated solvents, the ^{13}C NMR spectrum of **21j** was not successfully acquired. However, the ^{1}H NMR spectrum and HRMS data of **21j** afforded here could be the valid evidence

for the structure of **21j**. HRMS (ESI) *m/z*: calcd for $C_{25}H_{26}ClN_6O$ $[M+H]^+$ 461.1852, found 461.1855.

2-((2-((7-Bromo-1,2,3,4-tetrahydroacridin-9-yl)amino)ethyl)amino)-3-methyl-6-(pyridin-4-yl)pyrimidin-4(3*H*)-one (**21k**). White solid, 59% yield： Rf = 0.5 (10% methanol in dichloromethane). ^{1}H NMR (400 MHz, CD_3OD) δ 8.59 (dd, *J* = 4.6, 1.6 Hz, 2H), 8.43 (d, *J* = 1.7 Hz, 1H), 7.80 (ddd, *J* = 6.8, 6.2, 1.8 Hz, 3H), 7.48 (d, *J* = 9.0 Hz, 1H), 6.30 (s, 1H), 4.34 - 4.20 (m, 2H), 4.09 - 3.98 (m, 2H), 3.31 (s, 3H), 2.84 (t, *J* = 6.3 Hz, 2H), 2.61 (s, 2H), 1.88 - 1.69 (m, 4H). ^{13}C NMR (75 MHz, CD_3OD) Given the property of 300 MHz spectrometer and the low solubility of compound in deuterated solvents, the ^{13}C NMR spectrum of **21k** was not successfully acquired. However, the ^{1}H NMR spectrum and HRMS data of **21k** afforded here could be the valid evidence for the structure of **21k**. HRMS (ESI) *m/z*: calcd for $C_{25}H_{26}BrN_6O$ $[M+H]^+$ 505.1346, found 505.1346.

3-Methyl-6-(pyridin-4-yl)-2-((2-((7-(trifluoromethyl)-1,2,3,4-tetrahydroacridin-9-yl)amino)ethyl)amino)pyrimidin-4(3*H*)-one (**21l**). Brown solid, 64% yield：Rf = 0.4 (10% methanol in dichloromethane). ^{1}H NMR (300 MHz, CD_3OD) δ 8.52 (d, *J* = 18.9 Hz, 3H), 7.88 (d, *J* = 8.9 Hz, 1H), 7.80 - 7.68 (m, 3H), 6.30 (s, 1H), 4.25 (s, 2H), 4.01 (s, 2H), 3.33 (s, 3H), 2.87 (d, *J* = 5.7 Hz, 2H), 2.60 (s, 2H), 1.78 (m, 4H). ^{13}C NMR (75 MHz, CD_3OD) δ 167.9, 161.6, 160.0, 158.8, 157.9, 153.3, 153.3, 149.0, 145.6, 131.2, 130.4, 130.0, 129.8, 126.4, 124.9, 124.9, 120.1, 118.0, 102.5, 45.5, 33.3, 31.1, 31.1, 28.5, 25.5, 24.6. HRMS (ESI) *m/z*: calcd for $C_{26}H_{26}F_3N_6O$ $[M+H]^+$ 495.2115, found 495.2114.

3-Methyl-6-(pyridin-4-yl)-2-((2-((6-(trifluoromethyl)-1,2,3,4-tetrahydroacridin-9-yl)amino)ethyl)amino)pyrimidin-4(3*H*)-one (**21m**). Brown solid, 55% yield： Rf = 0.4 (10% methanol in dichloromethane). ^{1}H NMR (300 MHz, CD_3OD) δ 8.56 (d, *J* = 5.9 Hz, 2H), 8.23 (d, *J* = 8.9 Hz, 1H), 7.90 (s, 1H), 7.76 (d, *J* = 6.0 Hz, 2H), 7.32 (d, *J* = 8.7 Hz, 1H), 6.28 (s, 1H), 4.03 (s, 2H), 3.85 (s, 2H), 3.15 (s, 3H), 2.87 (d, *J* = 6.2 Hz, 2H), 2.65 (s, 2H), 1.77 (m, 4H). ^{13}C NMR (75 MHz, CD_3OD) δ 167.9, 162.9, 161.9, 158.7, 155.3, 153.2, 153.2, 149.2, 149.0, 133.9, 129.5, 128.4, 128.0, 125.0, 125.0, 124.7, 122.5, 120.6, 102.6, 46.0, 36.6, 30.9, 30.9, 28.9, 26.2, 25.8. HRMS (ESI) *m/z*: calcd for $C_{26}H_{26}F_3N_6O$ $[M+H]^+$ 495.2115, found 495.2116.

1-Methyl-2-((2-((1,2,3,4-tetrahydroacridin-9-yl)amino)ethyl)amino)-[4,4'-bipyrimidin]-6(1*H*)-one (**22a**). White solid, 65% yield：Rf = 0.4 (10% methanol in dichloromethane). ^{1}H NMR (300

MHz, CD_3OD) δ 9.19 (s, 1H), 8.76 (d, J = 5.1 Hz, 1H), 8.24 (d, J = 8.8 Hz, 1H), 7.83 (d, J = 5.0 Hz, 1H), 7.62 (d, J = 7.0 Hz, 2H), 7.35 (d, J = 6.7 Hz, 1H), 6.76 (s, 1H), 4.19 (s, 2H), 3.95 (s, 2H), 3.23 (s, 3H), 2.83 (s, 2H), 2.55 (s, 2H), 1.75 (m, 4H). ^{13}C NMR (75 MHz, DMSO-d_6) δ 162.7, 161.2, 159.0, 158.8, 156.3, 155.1, 155.0, 153.5, 143.1, 130.4, 124.5, 124.4, 118.9, 117.8, 114.9, 114.6, 98.6, 47.3, 31.4, 27.9, 27.9, 25.4, 22.6, 21.9. HRMS (ESI) *m/z*: calcd for $C_{24}H_{26}N_7O$ $[M+H]^+$ 428.2194, found 428.2201.

2-((2-((6-Fluoro-1,2,3,4-tetrahydroacridin-9-yl)amino)ethyl)amino)-1-methyl-[4,4'-bipyrimidin]-6(1*H*)-one (**22b**). White solid, 64% yield: Rf = 0.4 (10% methanol in dichloromethane). ^{1}H NMR (300 MHz, CD_3OD) δ 9.20 (s, 1H), 8.79 (d, J = 5.0 Hz, 1H), 8.46 - 8.29 (m, 1H), 7.89 (d, J = 5.0 Hz, 1H), 7.20 (dd, J = 20.5, 9.3 Hz, 2H), 6.76 (s, 1H), 4.26 (s, 2H), 4.00 (s, 2H), 3.29 (s, 3H), 2.80 (d, J = 5.3 Hz, 2H), 2.48 (s, 2H), 1.76 (d, J = 5.6 Hz, 4H). ^{13}C NMR (75 MHz, DMSO-d_6) δ 162.9, 161.7, 161.1, 160.8, 158.4, 158.3, 156.3, 155.2, 154.8, 117.6, 114.4, 114.1, 112.9, 112.6, 105.7, 103.5, 98.8, 29.7, 27.5, 27.5, 24.6, 21.9, 21.0, 20.0. HRMS (ESI) *m/z*: calcd for $C_{24}H_{25}FN_7O$ $[M+H]^+$ 446.2100, found 446.2105.

2-((2-((6-Chloro-1,2,3,4-tetrahydroacridin-9-yl)amino)ethyl)amino)-1-methyl-[4,4'-bipyrimidin]-6(1*H*)-one (**22c**). White solid, 57% yield: Rf = 0.5 (10% methanol in dichloromethane). ^{1}H NMR (300 MHz, CD_3OD) δ 9.23 (s, 1H), 8.79 (d, J = 5.3 Hz, 1H), 8.29 (d, J = 9.2 Hz, 1H), 7.89 (d, J = 5.2 Hz, 1H), 7.57 (d, J = 2.1 Hz, 1H), 7.33 (d, J = 9.0 Hz, 1H), 6.80 (s, 1H), 4.27 (s, 2H), 4.01 (s, 2H), 3.29 (s, 3H), 2.83 (d, J = 6.1 Hz, 2H), 2.51 (s, 2H), 1.77 (m, 4H). ^{13}C NMR (75 MHz, DMSO-d_6) δ 162.8, 161.2, 158.8, 158.6, 156.4, 154.8, 151.9, 146.4, 141.1, 133.7, 125.9, 125.6, 124.0, 118.4, 117.7, 116.0, 98.6, 42.3, 33.0, 27.5, 27.5, 25.4, 22.7, 22.3. HRMS (ESI) *m/z*: calcd for $C_{24}H_{25}ClN_7O$ $[M+H]^+$ 462.1804, found 462.1812.

2-((2-((6-Methoxy-1,2,3,4-tetrahydroacridin-9-yl)amino)ethyl)amino)-1-methyl-[4,4'-bipyrimidin]-6(1*H*)-one (**22d**). White solid, 61% yield: Rf = 0.5 (12.5% methanol in dichloromethane). ^{1}H NMR (300 MHz, CD_3OD) δ 9.23 (s, 1H), 8.77 (d, J = 5.1 Hz, 1H), 8.27 (d, J = 9.9 Hz, 1H), 7.88 (s, 1H), 7.01 (d, J = 9.6 Hz, 1H), 6.87 (s, 1H), 6.79 (s, 1H), 4.31 (s, 2H), 4.04 (s, 2H), 3.96 (s, 3H), 3.66 (s, 3H), 2.77 (s, 2H), 2.42 (s, 2H), 1.74 (m, 4H). ^{13}C NMR (75 MHz, CD_3OD) Given the property of 300 MHz spectrometer and the low solubility of compound in deuterated solvents, the ^{13}C NMR spectrum of **22d** was not successfully acquired. However, the ^{1}H NMR spectrum and HRMS data of **22d** afforded here could be the valid evidence for the structure

of **22d**. HRMS (ESI) *m/z*: calcd for $C_{25}H_{28}N_7O_2$ $[M+H]^+$ 458.2300, found 458.2303.

2-((2-((7-Chloro-1,2,3,4-tetrahydroacridin-9-yl)amino)ethyl)amino)-1-methyl-[4,4'-bipyrimidin]-6(1*H*)-one (**22e**). White solid, 60% yield: Rf = 0.4 (12.5% methanol in dichloromethane). ^{1}H NMR (300 MHz, CD_3OD) δ 9.19 (s, 1H), 8.81 (s, 1H), 8.11 (s, 1H), 7.92 (s, 1H), 7.51 (s, 2H), 6.72 (s, 1H), 4.12 (s, 2H), 3.89 (s, 2H), 3.20 (s, 3H), 2.86 (s, 2H), 2.67 (s, 2H), 1.81 (m, 4H). ^{13}C NMR (75 MHz, CD_3OD) Given the property of 300 MHz spectrometer and the low solubility of compound in deuterated solvents, the ^{13}C NMR spectrum of **22e** was not successfully acquired. However, the ^{1}H NMR spectrum and HRMS data of **22e** afforded here could be the valid evidence for the structure of **22e**. HRMS (ESI) *m/z*: calcd for $C_{24}H_{25}ClN_7O$ $[M+H]^+$ 462.1804, found 462.1809.

6-(3-Fluoropyridin-4-yl)-3-methyl-2-((2-((1,2,3,4-tetrahydroacridin-9-yl)amino)ethyl)amino)pyrimidin-4(3*H*)-one (**22f**). White solid, 65% yield: Rf = 0.4 (10% methanol in dichloromethane). ^{1}H NMR (300 MHz, CD_3OD) δ 8.56 (d, *J* = 3.4 Hz, 1H), 8.34 (dd, *J* = 9.3, 7.0 Hz, 2H), 7.82 - 7.70 (m, 2H), 7.59 (d, *J* = 7.8 Hz, 1H), 7.43 (t, *J* = 7.8 Hz, 1H), 6.32 (d, *J* = 1.2 Hz, 1H), 4.37 - 4.25 (m, 2H), 4.10 - 3.98 (m, 2H), 3.33 (s, 3H), 2.86 (t, *J* = 5.9 Hz, 2H), 2.51 (t, *J* = 5.7 Hz, 2H), 1.81 (m, 4H). ^{13}C NMR (75 MHz, CD_3OD) δ 163.6, 156.8, 154.9, 153.6, 150.2, 145.5, 139.0, 138.6, 138.3, 132.8, 132.7, 125.2, 124.8, 123.6, 119.1, 116.0, 111.8, 103.6, 41.3, 28.0, 27.5, 27.5, 24.1, 21.5, 20.5. HRMS (ESI) *m/z*: calcd for $C_{25}H_{26}FN_6O$ $[M+H]^+$ 445.2147, found 445.2146.

2-((2-((6-Fluoro-1,2,3,4-tetrahydroacridin-9-yl)amino)ethyl)amino)-6-(3-fluoropyridin-4-yl)-3-methylpyrimidin-4(3*H*)-one (**22g**). White solid, 70% yield: Rf = 0.4 (10% methanol in dichloromethane). ^{1}H NMR (300 MHz, CD_3OD) δ 8.58 (d, *J* = 3.1 Hz, 1H), 8.43 - 8.29 (m, 2H), 7.76 (t, *J* = 5.9 Hz, 1H), 7.31 - 7.09 (m, 2H), 6.34 (s, 1H), 4.19 (d, *J* = 5.1 Hz, 2H), 3.99 (t, *J* = 5.1 Hz, 2H), 3.32 (s, 3H), 2.86 (t, *J* = 5.8 Hz, 2H), 2.54 (d, *J* = 5.8 Hz, 2H), 1.81 (m, 4H). ^{13}C NMR (75 MHz, CD_3OD) δ 165.3, 163.6, 161.9, 154.9, 153.6, 153.3, 145.6, 142.5, 139.0, 138.6, 132.7, 127.3, 123.5, 114.4, 114.1, 112.6, 106.1, 103.7, 41.4, 29.6, 27.5, 27.5, 24.1, 21.8, 20.9. HRMS (ESI) *m/z*: calcd for $C_{25}H_{25}F_2N_6O$ $[M+H]^+$ 463.2053, found 463.2051.

2-((2-((6-Chloro-1,2,3,4-tetrahydroacridin-9-yl)amino)ethyl)amino)-6-(3-fluoropyridin-4-yl)-3-methylpyrimidin-4(3*H*)-one (**22h**). White solid, 68% yield: Rf = 0.5 (10% methanol in dichloromethane). ^{1}H NMR (300 MHz, CD_3OD) δ 8.58 (d, *J* = 3.0 Hz, 1H), 8.36 (d, *J* = 5.0 Hz, 1H), 8.25 (d, *J* = 9.2 Hz, 1H), 7.72 (t, *J* = 5.8 Hz, 1H), 7.55 (s, 1H), 7.29 (d, *J* = 9.0 Hz, 1H), 6.33

(s, 1H), 4.20 (d, *J* = 4.9 Hz, 2H), 3.99 (d, *J* = 5.3 Hz, 2H), 3.32 (s, 3H), 2.85 (d, *J* = 5.7 Hz, 2H), 2.53 (s, 2H), 1.81 (m, 4H). ^{13}C NMR (75 MHz, CD_3OD) δ 163.6, 158.9, 155.0, 154.8, 153.7, 153.0, 145.5, 141.3, 139.0, 138.6, 137.5, 126.1, 125.2, 123.6, 120.4, 115.3, 113.1, 103.6, 41.4, 29.5, 27.5, 27.5, 24.2, 21.7, 20.9. HRMS (ESI) *m/z*: calcd for $C_{25}H_{25}FClN_6O$ $[M+H]^+$ 479.1759, found 479.1760.

6-(3-Fluoropyridin-4-yl)-2-((2-((6-methoxy-1,2,3,4-tetrahydroacridin-9-yl)amino)ethyl)amino)-3-methylpyrimidin-4(3*H*)-one (**22i**). White solid, 67% yield: Rf = 0.5 (10% methanol in dichloromethane). ^{1}H NMR (300 MHz, CD_3OD) δ 8.57 (s, 1H), 8.37 (d, *J* = 5.0 Hz, 1H), 8.06 (d, *J* = 9.3 Hz, 1H), 7.74 (t, *J* = 5.8 Hz, 1H), 7.00 - 6.80 (m, 2H), 6.34 (s, 1H), 4.17 - 4.00 (m, 2H), 3.96 - 3.82 (m, 5H), 3.26 (s, 3H), 2.94 - 2.67 (m, 2H), 2.54 (s, 2H), 1.81 (m, 4H). ^{13}C NMR (75 MHz, CD_3OD) δ 163.7, 161.0, 159.0, 154.6, 154.1, 153.7, 153.4, 145.5, 145.2, 138.9, 138.5, 132.7, 125.1, 123.6, 116.3, 112.7, 112.5, 102.4, 55.2, 41.8, 30.7, 29.5, 27.3, 24.2, 22.2, 21.5. HRMS (ESI) *m/z*: calcd for $C_{26}H_{28}FN_6O_2$ $[M+H]^+$ 474.2253, found 475.2247.

2-((2-((7-Chloro-1,2,3,4-tetrahydroacridin-9-yl)amino)ethyl)amino)-6-(3-fluoropyridin-4-yl)-3-methylpyrimidin-4(3*H*)-one (**22j**). White solid, 62% yield: Rf = 0.5 (10% methanol in dichloromethane). ^{1}H NMR (300 MHz, CD_3OD) δ 8.56 (d, *J* = 3.1 Hz, 1H), 8.42 (d, *J* = 4.9 Hz, 1H), 8.07 (s, 1H), 7.81 (t, *J* = 5.9 Hz, 1H), 7.61 (d, *J* = 9.0 Hz, 1H), 7.47 (d, *J* = 8.9 Hz, 1H), 6.32 (s, 1H), 4.01 (d, *J* = 5.2 Hz, 2H), 3.85 (d, *J* = 5.4 Hz, 2H), 3.21 (s, 3H), 2.96 - 2.80 (m, 2H), 2.73 (d, *J* = 5.6 Hz, 2H), 1.84 (m, 4H). ^{13}C NMR (75 MHz, CD_3OD) δ 163.8, 156.9, 154.5, 153.7, 151.6, 145.4, 143.1, 138.9, 138.6, 132.7, 130.0, 129.6, 127.2, 123.6, 122.1, 119.9, 116.1, 103.6, 42.1, 31.9, 27.2, 27.2, 25.0, 22.3, 21.9. HRMS (ESI) *m/z*: calcd for $C_{25}H_{25}FClN_6O$ $[M+H]^+$ 479.1757, found 479.1763.

3-Methyl-6-(pyridin-4-yl)-2-((3-((1,2,3,4-tetrahydroacridin-9-yl)amino)propyl)amino)pyrimidin-4(3*H*)-one (**23a**). Yellow solid, 59% yield: Rf = 0.4 (10% methanol in dichloromethane). ^{1}H NMR (300 MHz, CD_3OD) δ 8.52 (d, *J* = 4.3 Hz, 2H), 8.22 (d, *J* = 8.3 Hz, 1H), 7.79 (d, *J* = 4.6 Hz, 2H), 7.68 - 7.57 (m, 1H), 7.52 (d, *J* = 8.1 Hz, 1H), 7.35 (t, *J* = 7.4 Hz, 1H), 6.28 (s, 1H), 4.10 (s, 2H), 3.74 (s, 2H), 3.31 (s, 3H), 2.77 (s, 2H), 2.60 (s, 2H), 2.23 (s, 2H), 1.79 (m, 4H). ^{13}C NMR (75 MHz, CD_3OD) δ 164.2, 157.8, 155.5, 154.4, 151.3, 149.3, 149.3, 145.3, 139.7, 131.9, 124.7, 124.4, 121.1, 121.1, 120.3, 116.3, 111.9, 97.9, 39.4, 29.9, 28.8, 27.4, 27.4, 24.1, 21.8, 20.8. HRMS (ESI) *m/z*: calcd for $C_{26}H_{29}N_6O$ $[M+H]^+$ 441.2398, found 441.2407.

3-Methyl-6-(pyridin-4-yl)-2-((4-((1,2,3,4-tetrahydroacridin-9-yl)amino)butyl)amino)pyrimidin-4(3*H*)-one (**23b**). Yellow solid, 63% yield: Rf = 0.4 (10% methanol in dichloromethane). ^{1}H NMR (300 MHz, CD_3OD) δ 8.56 (d, *J* = 4.6 Hz, 2H), 8.28 (d, *J* = 8.5 Hz, 1H), 7.90 (d, *J* = 4.4 Hz, 2H), 7.72 (q, *J* = 8.4 Hz, 2H), 7.43 (t, *J* = 7.5 Hz, 1H), 6.34 (s, 1H), 3.96 (d, *J* = 6.4 Hz, 2H), 3.61 (s, 2H), 3.25 (s, 3H), 2.87 (s, 2H), 2.58 (s, 2H), 2.02 - 1.71 (m, 8H). ^{13}C NMR (75 MHz, CD_3OD) δ 164.4, 157.9, 155.9, 154.5, 151.5, 149.5, 149.5, 145.6, 139.9, 132.2, 125.0, 124.8, 121.3, 121.3, 120.4, 116.5, 112.3, 97.5, 41.6, 28.9, 27.7, 26.8, 26.8, 25.6, 23.9, 21.9, 20.9. HRMS (ESI) *m/z*: calcd for $C_{27}H_{31}N_6O$ $[M+H]^+$ 455.2554, found 455.2562.

3-Methyl-6-(pyridin-4-yl)-2-((5-((1,2,3,4-tetrahydroacridin-9-yl)amino)pentyl)amino)pyrimidin-4(3*H*)-one (**23c**). Yellow solid, 57% yield: Rf = 0.5 (10% methanol in dichloromethane). ^{1}H NMR (300 MHz, CD_3OD) δ 8.51 (d, *J* = 4.7 Hz, 2H), 8.21 (d, *J* = 8.5 Hz, 1H), 7.84 (d, *J* = 4.7 Hz, 2H), 7.70 - 7.59 (m, 2H), 7.39 (t, *J* = 7.5 Hz, 1H), 6.31 (s, 1H), 3.83 (t, *J* = 6.7 Hz, 2H), 3.59 (t, *J* = 6.5 Hz, 2H), 3.33 (d, *J* = 6.3 Hz, 3H), 2.90 (s, 2H), 2.62 (s, 2H), 1.87 (m, 6H), 1.79 - 1.68 (m, 2H), 1.55 (d, *J* = 6.5 Hz, 2H). ^{13}C NMR (75 MHz, CD_3OD) δ 164.5, 158.0, 155.3, 154.7, 152.3, 149.4, 149.4, 145.7, 140.6, 131.8, 124.7, 124.7, 121.2, 121.2, 121.0, 116.8, 112.5, 97.4, 41.5, 30.2, 29.4, 28.6, 26.9, 26.9, 24.2, 23.7, 22.1, 21.2. HRMS (ESI) *m/z*: calcd for $C_{28}H_{33}N_6O$ $[M+H]^+$ 469.2711, found 469.2704.

3-Methyl-6-(pyridin-4-yl)-2-((6-((1,2,3,4-tetrahydroacridin-9-yl)amino)hexyl)amino)pyrimidin-4(3*H*)-one (**23d**). Yellow solid, 53% yield: Rf = 0.5 (10% methanol in dichloromethane). ^{1}H NMR (300 MHz, CD_3OD) δ 8.57 (d, *J* = 4.3 Hz, 2H), 8.35 (d, *J* = 8.6 Hz, 1H), 7.94 (d, *J* = 4.4 Hz, 2H), 7.87 - 7.71 (m, 2H), 7.54 (t, *J* = 7.6 Hz, 1H), 6.38 (s, 1H), 3.94 (t, *J* = 7.0 Hz, 2H), 3.60 (t, *J* = 6.6 Hz, 2H), 3.40 (s, 3H), 2.99 (s, 2H), 2.66 (s, 2H), 1.91 (m, 6H), 1.77 (s, 2H), 1.54 (m, 4H). ^{13}C NMR (75 MHz, CD_3OD) δ 164.6, 158.3, 156.7, 154.7, 150.4, 149.4, 149.4, 145.9, 138.6, 132.9, 125.4, 125.2, 125.2, 121.4, 119.0, 115.8, 111.6, 97.5, 41.88, 30.3, 29.0, 28.2, 27.0, 27.0, 26.4, 26.4, 23.8, 21.8, 20.7. HRMS (ESI) *m/z*: calcd for $C_{29}H_{35}N_6O$ $[M+H]^+$ 483.2867, found 483.2862.

3-Methyl-6-(pyridin-4-yl)-2-((7-((1,2,3,4-tetrahydroacridin-9-yl)amino)heptyl)amino)pyrimidin-4(3*H*)-one (**23e**). Yellow solid, 63% yield: Rf = 0.6 (9% methanol in dichloromethane). ^{1}H NMR (300 MHz, CD_3OD) δ 8.55 (d, *J* = 5.0 Hz, 2H), 8.31 (d, *J* = 8.8 Hz, 1H), 7.92 (d, *J* = 4.9 Hz, 2H), 7.80 (t, *J* = 7.6 Hz, 1H), 7.71 (d, *J* = 8.3 Hz, 1H), 7.51 (t, *J* = 7.8 Hz, 1H), 6.35 (s, 1H), 3.89 (t, *J* = 6.9 Hz, 2H), 3.57 (t, *J* = 6.9 Hz, 2H), 3.39 (s, 3H), 2.98 (s,

2H), 2.63 (s, 2H), 1.93 (m, 4H), 1.82 (s, 2H), 1.72 (s, 2H), 1.46 (m, 6H). ^{13}C NMR (75 MHz, CD_3OD) δ 164.7, 158.4, 154.5, 154.3, 153.7, 149.3, 149.3, 145.9, 142.3, 130.9, 124.4, 124.2, 122.7, 121.3, 121.3, 117.7, 113.3, 97.6, 41.9, 30.8, 30.4, 29.5, 29.0, 28.9, 27.1, 26.7, 26.7, 24.1, 22.3, 21.5. HRMS (ESI) *m/z*: calcd for $C_{30}H_{37}N_6O$ $[M+H]^+$ 497.3024, found 497.3017.

2-((6-((6-Bromo-1,2,3,4-tetrahydroacridin-9-yl)amino)hexyl)amino)-3-methyl-6-(pyridin-4-yl)pyrimidin-4(3*H*)-one (**26a**). Yellow solid, 60% yield: Rf = 0.5 (10% methanol in dichloromethane). ^{1}H NMR (300 MHz, CD_3OD) δ 8.59 (d, J = 5.4 Hz, 2H), 8.00 (d, J = 9.1 Hz, 1H), 7.94 (d, J = 5.3 Hz, 2H), 7.89 (s, 1H), 7.41 (d, J = 9.2 Hz, 1H), 6.39 (s, 1H), 3.65 - 3.49 (m, 4H), 3.40 (s, 3H), 2.94 (s, 2H), 2.66 (s, 2H), 1.88 (s, 4H), 1.71 (s, 4H), 1.46 (m, 4H). ^{13}C NMR (75 MHz, CD_3OD) δ 164.6, 158.3, 157.8, 154.4, 152.3, 149.2, 149.2, 146.5, 145.8, 128.1, 126.7, 125.2, 123.1, 121.2, 121.2, 117.8, 115.0, 97.6, 48.7, 41.9, 32.4, 31.1, 29.0, 27.0, 26.5, 26.5, 24.5, 22.5, 22.0. HRMS (ESI) *m/z*: calcd for $C_{29}H_{34}BrN_6O$ $[M+H]^+$ 561.1972, found 561.1984.

2-((6-((6-Chloro-1,2,3,4-tetrahydroacridin-9-yl)amino)hexyl)amino)-3-methyl-6-(pyridin-4-yl)pyrimidin-4(3*H*)-one (**26b**). Yellow solid, 68% yield: Rf = 0.5 (10% methanol in dichloromethane). ^{1}H NMR (300 MHz, CD_3OD) δ 8.59 (d, J = 5.3 Hz, 2H), 8.16 (d, J = 9.2 Hz, 1H), 7.95 (d, J = 5.1 Hz, 2H), 7.71 (s, 1H), 7.36 (d, J = 9.1 Hz, 1H), 6.40 (s, 1H), 3.70 (t, J = 7.2 Hz, 2H), 3.58 (t, J = 6.9 Hz, 2H), 3.41 (s, 3H), 2.95 (s, 2H), 2.66 (s, 2H), 1.91 (s, 4H), 1.76 (d, J = 6.1 Hz, 4H), 1.50 (m, 4H). ^{13}C NMR (75 MHz, CD_3OD) δ 164.6, 158.3, 155.5, 154.4, 153.5, 149.2, 149.2, 145.8, 144.0, 136.2, 125.8, 124.6, 122.6, 121.2, 121.2, 116.4, 114.0, 97.6, 48.4, 41.8, 31.0, 30.8, 28.9, 27.0, 26.5, 26.4, 24.1, 22.2, 21.5. HRMS (ESI) *m/z*: calcd for $C_{29}H_{34}ClN_6O$ $[M+H]^+$ 517.2478, found 517.2479.

2-((6-((6-Fluoro-1,2,3,4-tetrahydroacridin-9-yl)amino)hexyl)amino)-3-methyl-6-(pyridin-4-yl)pyrimidin-4(3*H*)-one (**26c**). Yellow solid, 67% yield: Rf = 0.4 (10% methanol in dichloromethane). ^{1}H NMR (300 MHz, CD_3OD) δ 8.60 (d, J = 5.9 Hz, 2H), 8.29 (dd, J = 9.3, 5.8 Hz, 1H), 7.96 (d, J = 5.9 Hz, 2H), 7.38 (d, J = 9.8 Hz, 1H), 7.25 (t, J = 8.7 Hz, 1H), 6.40 (s, 1H), 3.75 (t, J = 7.1 Hz, 2H), 3.59 (t, J = 7.0 Hz, 2H), 3.41 (s, 3H), 2.96 (s, 2H), 2.66 (s, 2H), 1.93 (d, J = 11.5 Hz, 4H), 1.87 - 1.65 (m, 4H), 1.48 (m, 4H). ^{13}C NMR (75 MHz, CD_3OD) δ 164.6, 162.3, 158.3, 154.6, 154.4, 154.1, 149.2, 149.2, 145.8, 144.1, 127.2, 121.3, 121.3, 114.6, 113.9, 113.0, 107.5, 97.6, 48.4, 41.8, 30.7, 30.4, 28.9, 27.1, 26.5, 26.4, 23.9, 22.2, 21.4. HRMS (ESI) *m/z*: calcd for $C_{29}H_{34}FN_6O$ $[M+H]^+$ 501.2773, found 501.2780.

2-((6-((7-Fluoro-1,2,3,4-tetrahydroacridin-9-yl)amino)hexyl)amino)-3-methyl-6-(pyridin-4-yl)pyrimidin-4(3*H*)-one (**26d**). Brown solid, 64% yield: Rf = 0.4 (10% methanol in dichloromethane). ^{1}H NMR (300 MHz, CD_3OD) δ 8.59 (d, J = 4.9 Hz, 2H), 7.95 (d, J = 4.9 Hz, 2H), 7.80 (d, J = 9.4 Hz, 2H), 7.43 (t, J = 8.4 Hz, 1H), 6.39 (s, 1H), 3.56 (s, 4H), 3.40 (s, 3H), 2.97 (s, 2H), 2.72 (s, 2H), 1.90 (s, 4H), 1.72 (s, 4H), 1.48 (s, 4H). ^{13}C NMR (75 MHz, CD_3OD) δ 164.6, 160.1, 158.3, 156.3, 154.4, 152.0, 149.2, 149.2, 145.8, 142.1, 128.0, 121.2, 121.2, 119.9, 119.2, 115.7, 107.0, 97.6, 48.3, 41.8, 32.0, 31.0, 29.0, 27.0, 26.5, 26.5, 24.6, 22.5, 22.0. HRMS (ESI) *m/z*: calcd for $C_{29}H_{34}FN_6O$ $[M+H]^+$ 501.2773, found 501.2780.

3-Methyl-2-((6-((6-methyl-1,2,3,4-tetrahydroacridin-9-yl)amino)hexyl)amino)-6-(pyridin-4-yl)pyrimidin-4(3*H*)-one (**26e**). Yellow solid, 62% yield: Rf = 0.5 (10% methanol in dichloromethane). ^{1}H NMR (300 MHz, CD_3OD) δ 8.59 (d, J = 5.8 Hz, 2H), 8.24 (d, J = 8.8 Hz, 1H), 7.95 (d, J = 5.8 Hz, 2H), 7.51 (s, 1H), 7.38 (d, J = 8.9 Hz, 1H), 6.39 (s, 1H), 3.94 (t, J = 7.1 Hz, 2H), 3.62 (t, J = 6.8 Hz, 2H), 3.42 (s, 3H), 2.98 (s, 2H), 2.63 (s, 2H), 2.56 (s, 3H), 1.92 (m, 6H), 1.81 (d, J = 6.4 Hz, 2H), 1.57 (m, 4H). ^{13}C NMR (75 MHz, CD_3OD) δ 164.6, 158.3, 156.2, 154.5, 149.5, 149.2, 149.2, 145.8, 144.3, 138.8, 127.1, 124.9, 121.2, 121.2, 118.1, 113.7, 111.0, 97.6, 47.8, 41.8, 30.3, 28.9, 28.0, 27.1, 26.4, 26.3, 23.4, 21.8, 21.0, 20.6. HRMS (ESI) *m/z*: calcd for $C_{30}H_{37}N_6O$ $[M+H]^+$ 497.3024, found 497.3027.

2-((6-((6-Bromo-1,2,3,4-tetrahydroacridin-9-yl)amino)hexyl)amino)-6-(3-fluoropyridin-4-yl)-3-methylpyrimidin-4(3*H*)-one (**26f**). Yellow solid, 68% yield: Rf = 0.5 (10% methanol in dichloromethane). ^{1}H NMR (300 MHz, CD_3OD) δ 8.52 (d, J = 3.2 Hz, 1H), 8.42 (d, J = 4.9 Hz, 1H), 8.02 (t, J = 7.4 Hz, 2H), 7.89 (s, 1H), 7.42 (d, J = 9.1 Hz, 1H), 6.42 (s, 1H), 3.55 (dt, J = 20.2, 7.1 Hz, 4H), 3.40 (s, 3H), 2.95 (s, 2H), 2.68 (s, 2H), 1.89 (s, 4H), 1.70 (s, 4H), 1.42 (m, 4H). ^{13}C NMR (75 MHz, CD_3OD) δ 164.3, 158.8, 158.1, 156.2, 154.2, 152.1, 146.7, 145.3, 138.8, 133.2, 128.3, 126.7, 125.1, 123.9, 123.0, 117.9, 115.1, 102.7, 48.8, 41.9, 32.5, 31.2, 29.0, 27.1, 26.6, 26.5, 24.5, 22.5, 22.1. HRMS (ESI) *m/z*: calcd for $C_{29}H_{33}BrFN_6O$ $[M+H]^+$ 579.1878, found 579.1884.

2-((6-((6-Chloro-1,2,3,4-tetrahydroacridin-9-yl)amino)hexyl)amino)-6-(3-fluoropyridin-4-yl)-3-methylpyrimidin-4(3*H*)-one (**26g**). Yellow solid, 63% yield: Rf = 0.5 (10% methanol in dichloromethane). ^{1}H NMR (300 MHz, CD_3OD) δ 8.52 (d, J = 3.3 Hz, 1H), 8.42 (d, J = 5.0 Hz, 1H), 8.14 (d, J = 9.1 Hz, 1H), 8.03 (t, J = 5.9 Hz, 1H), 7.71 (s, 1H), 7.34 (d, J = 9.1 Hz, 1H), 6.41 (s, 1H), 3.67 (t, J = 7.1 Hz, 2H), 3.54 (t, J = 7.0 Hz, 2H), 3.41 (s, 3H), 2.96 (s, 2H), 2.68 (s, 2H),

1.93 (d, *J* = 12.1 Hz, 4H), 1.74 (d, *J* = 5.8 Hz, 4H), 1.49 (m, 4H). ^{13}C NMR (75 MHz, CD_3OD) δ 164.3, 158.8, 156.4, 154.2, 153.0, 145.3, 144.8, 138.8, 138.5, 135.8, 133.2, 125.5, 124.6, 123.9, 123.5, 116.8, 114.3, 102.8, 48.6, 41.9, 31.5, 31.0, 28.9, 27.1, 26.5, 26.5, 24.2, 22.3, 21.8. HRMS (ESI) *m/z*: calcd for $C_{29}H_{33}ClFN_6O$ $[M+H]^+$ 535.2383, found 535.2390.

2-((6-((6-Fluoro-1,2,3,4-tetrahydroacridin-9-yl)amino)hexyl)amino)-6-(3-fluoropyridin-4-yl)-3-methylpyrimidin-4(3*H*)-one (**26h**). Yellow solid, 68% yield: Rf = 0.4 (10% methanol in dichloromethane). ^{1}H NMR (300 MHz, CD_3OD) δ 8.53 (d, *J* = 3.3 Hz, 1H), 8.43 (d, *J* = 4.8 Hz, 1H), 8.35 (dd, *J* = 9.4, 5.6 Hz, 1H), 8.05 (t, *J* = 5.9 Hz, 1H), 7.40 (d, *J* = 9.6 Hz, 1H), 7.30 (t, *J* = 8.8 Hz, 1H), 6.41 (s, 1H), 3.82 (t, *J* = 7.1 Hz, 2H), 3.57 (t, *J* = 7.0 Hz, 2H), 3.42 (s, 3H), 2.98 (s, 2H), 2.66 (s, 2H), 1.94 (s, 4H), 1.80 (dd, *J* = 16.4, 7.0 Hz, 4H), 1.53 (m, 4H). ^{13}C NMR (75 MHz, CD_3OD) δ 165.1, 164.3, 162.6, 158.8, 156.2, 155.0, 154.2, 153.2, 145.3, 142.8, 138.7, 133.2, 127.8, 123.8, 114.1, 112.4, 105.7, 102.4, 48.3, 41.8, 30.5, 29.6, 28.8, 27.1, 26.4, 26.4, 23.7, 22.0, 21.0. HRMS (ESI) *m/z*: calcd for $C_{29}H_{33}F_2N_6O$ $[M+H]^+$ 519.2679, found 519.2684.

2-((6-((7-Fluoro-1,2,3,4-tetrahydroacridin-9-yl)amino)hexyl)amino)-6-(3-fluoropyridin-4-yl)-3-methylpyrimidin-4(3*H*)-one (**26i**). Brown solid, 60% yield: Rf = 0.4 (10% methanol in dichloromethane). ^{1}H NMR (300 MHz, CD_3OD) δ 8.52 (s, 1H), 8.43 (d, *J* = 4.8 Hz, 1H), 8.05 (d, *J* = 5.4 Hz, 1H), 7.81 (dd, *J* = 18.7, 8.9 Hz, 2H), 7.48 (t, *J* = 8.2 Hz, 1H), 6.41 (s, 1H), 3.62 (t, *J* = 7.1 Hz, 2H), 3.55 (t, *J* = 6.8 Hz, 2H), 3.41 (s, 3H), 2.99 (s, 2H), 2.73 (s, 2H), 1.92 (s, 4H), 1.74 (d, *J* = 5.7 Hz, 4H), 1.44 (d, *J* = 27.9 Hz, 4H). ^{13}C NMR (75 MHz, CD_3OD) δ 164.3, 160.1, 158.8, 157.7, 156.2, 155.2, 154.2, 152.7, 145.3, 140.8, 138.7, 133.1, 126.9, 123.8, 119.5, 114.9, 107.4, 102.6, 48.2, 41.8, 31.3, 30.9, 28.9, 27.0, 26.5, 26.4, 24.5, 22.4, 21.7. HRMS (ESI) *m/z*: calcd for $C_{29}H_{33}F_2N_6O$ $[M+H]^+$ 519.2679, found 519.2680.

6-(3-Fluoropyridin-4-yl)-3-methyl-2-((6-((1,2,3,4-tetrahydroacridin-9-yl)amino)hexyl)amino)pyrimidin-4(3*H*)-one (**26j**). Yellow solid, 63% yield: Rf = 0.4 (10% methanol in dichloromethane). ^{1}H NMR (300 MHz, CD_3OD) δ 8.53 (s, 1H), 8.43 (d, *J* = 4.7 Hz, 1H), 8.31 (d, *J* = 8.6 Hz, 1H), 8.05 (t, *J* = 5.8 Hz, 1H), 7.77 (s, 2H), 7.52 (d, *J* = 6.3 Hz, 1H), 6.41 (s, 1H), 3.87 (t, *J* = 7.1 Hz, 2H), 3.57 (t, *J* = 6.9 Hz, 2H), 3.42 (s, 3H), 3.01 (s, 2H), 2.69 (s, 2H), 1.96 (s, 4H), 1.81 (d, *J* = 28.3 Hz, 4H), 1.53 (m, 4H). ^{13}C NMR (75 MHz, CD_3OD) δ 164.3, 158.8, 156.2, 155.5, 154.2, 151.6, 145.3, 140.1, 138.7, 133.1, 131.9, 124.8, 124.6, 123.8, 120.6, 116.5, 112.2, 102.6, 48.1, 41.8, 30.5, 29.0, 28.8, 27.1, 26.4, 26.3, 23.8, 21.9, 20.9. HRMS (ESI) *m/z*: calcd

for $C_{29}H_{34}FN_6O$ $[M+H]^+$ 501.2773, found 501.2779.

6-(3-Fluoropyridin-4-yl)-3-methyl-2-((6-((6-methyl-1,2,3,4-tetrahydroacridin-9-yl)amino)hexyl)amino)pyrimidin-4(3*H*)-one (**26k**). Yellow solid, 62% yield: Rf = 0.5 (10% methanol in dichloromethane). ^{1}H NMR (300 MHz, CD_3OD) δ 8.51 (d, J = 3.3 Hz, 1H), 8.41 (d, J = 4.9 Hz, 1H), 8.04 (dt, J = 16.3, 9.3 Hz, 2H), 7.52 (s, 1H), 7.27 (d, J = 8.7 Hz, 1H), 6.36 (d, J = 19.6 Hz, 1H), 3.72 (t, J = 7.1 Hz, 2H), 3.54 (t, J = 7.0 Hz, 2H), 3.40 (s, 3H), 2.96 (s, 2H), 2.66 (s, 2H), 2.51 (s, 3H), 1.88 (d, J = 22.5 Hz, 4H), 1.84 - 1.65 (m, 4H), 1.50 (m, 4H). ^{13}C NMR (75 MHz, CD_3OD) δ 164.3, 158.8, 156.2, 154.2, 154.0, 153.4, 145.3, 142.7, 141.6, 138.7, 138.5, 133.1, 126.4, 123.8, 121.9, 115.7, 112.7, 102.6, 48.3, 41.8, 30.8, 30.4, 28.9, 27.1, 26.5, 26.4, 24.0, 22.3, 21.5, 20.9. HRMS (ESI) *m/z*: calcd for $C_{30}H_{36}FN_6O$ $[M+H]^+$ 515.2930, found 515.2934.

2-((7-((6-Bromo-1,2,3,4-tetrahydroacridin-9-yl)amino)heptyl)amino)-3-methyl-6-(pyridin-4-yl)pyrimidin-4(3*H*)-one (**27a**). Yellow solid, 61% yield: Rf = 0.6 (10% methanol in dichloromethane). ^{1}H NMR (300 MHz, CD_3OD) δ 8.60 (s, 2H), 8.02 (d, J = 8.8 Hz, 1H), 7.93 (d, J = 15.4 Hz, 3H), 7.44 (d, J = 8.7 Hz, 1H), 6.42 (s, 1H), 3.69 - 3.48 (m, 4H), 3.43 (s, 3H), 2.96 (s, 2H), 2.68 (s, 2H), 1.92 (s, 4H), 1.71 (s, 4H), 1.38 (m, 6H). ^{13}C NMR (75 MHz, CD_3OD) δ 164.6, 158.4, 157.4, 154.4, 152.5, 149.3, 149.3, 146.1, 145.8, 127.7, 126.8, 125.3, 123.4, 121.3, 121.3, 117.6, 114.8, 97.7, 48.7, 42.0, 32.2, 31.1, 29.0, 28.9, 27.0, 26.7, 26.7, 24.4, 22.5, 22.0. HRMS (ESI) *m/z*: calcd for $C_{30}H_{36}BrN_6O$ $[M+H]^+$ 575.2129, found 575.2134.

2-((7-((6-Chloro-1,2,3,4-tetrahydroacridin-9-yl)amino)heptyl)amino)-3-methyl-6-(pyridin-4-yl)pyrimidin-4(3*H*)-one (**27b**). Yellow solid, 62% yield: Rf = 0.6 (10% methanol in dichloromethane). ^{1}H NMR (300 MHz, CD_3OD) δ 8.61 (d, J = 4.4 Hz, 2H), 8.16 (d, J = 9.3 Hz, 1H), 7.97 (d, J = 4.5 Hz, 2H), 7.73 (s, 1H), 7.38 (d, J = 9.2 Hz, 1H), 6.41 (s, 1H), 3.69 (t, J = 6.8 Hz, 2H), 3.58 (t, J = 6.9 Hz, 2H), 3.44 (s, 3H), 2.97 (s, 2H), 2.69 (s, 2H), 1.93 (s, 4H), 1.73 (s, 4H), 1.46 (m, 6H). ^{13}C NMR (75 MHz, CD_3OD) δ 164.6, 158.3, 155.3, 154.4, 153.6, 149.2, 149.2, 145.8, 143.8, 136.3, 125.8, 124.6, 122.4, 121.3, 121.3, 116.3, 113.8, 97.6, 48.4, 41.9, 30.9, 30.8, 28.9, 28.9, 27.0, 26.7, 26.6, 24.1, 22.2, 21.5. HRMS (ESI) *m/z*: calcd for $C_{30}H_{36}ClN_6O$ $[M+H]^+$ 531.2634, found 531.2642.

2-((7-((6-Fluoro-1,2,3,4-tetrahydroacridin-9-yl)amino)heptyl)amino)-3-methyl-6-(pyridin-4-yl)pyrimidin-4(3*H*)-one (**27c**). Yellow solid, 63% yield: Rf = 0.5 (10% methanol in dichloromethane). ^{1}H NMR (300 MHz, CD_3OD) δ 8.61 (d, J = 4.8 Hz, 2H), 8.25 - 8.15 (m, 1H),

7.97 (d, *J* = 4.9 Hz, 2H), 7.37 (d, *J* = 10.4 Hz, 1H), 7.21 (t, *J* = 8.3 Hz, 1H), 6.42 (s, 1H), 3.61 (dt, *J* = 19.0, 7.0 Hz, 4H), 3.43 (s, 3H), 2.97 (s, 2H), 2.69 (s, 2H), 1.92 (s, 4H), 1.72 (s, 4H), 1.42 (m, 6H). ^{13}C NMR (75 MHz, CD_3OD) δ 164.6, 164.3, 161.8, 158.3, 156.8, 154.4, 153.0, 149.2, 149.2, 145.8, 126.5, 121.3, 121.3, 115.6, 113.8, 113.4, 108.6, 97.6, 48.7, 41.9, 31.7, 30.9, 28.9, 28.9, 27.0, 26.7, 26.6, 24.2, 22.4, 21.8. HRMS (ESI) *m/z*: calcd for $C_{30}H_{36}FN_6O$ $[M+H]^+$ 515.2930, found 515.2939.

2-((7-((7-Fluoro-1,2,3,4-tetrahydroacridin-9-yl)amino)heptyl)amino)-3-methyl-6-(pyridin-4-yl)pyrimidin-4(3*H*)-one (**27d**). Yellow solid, 60% yield: Rf = 0.5 (10% methanol in dichloromethane). ^{1}H NMR (300 MHz, CD_3OD) δ 8.61 (d, *J* = 5.8 Hz, 2H), 7.96 (d, *J* = 5.8 Hz, 2H), 7.80 (d, *J* = 9.7 Hz, 1H), 7.45 (t, *J* = 8.6 Hz, 1H), 6.40 (s, 1H), 3.57 (s, 4H), 3.43 (s, 3H), 2.99 (s, 2H), 2.74 (s, 2H), 1.86 (d, *J* = 36.9 Hz, 4H), 1.71 (d, *J* = 5.7 Hz, 4H), 1.42 (m, 6H). ^{13}C NMR (75 MHz, CD_3OD) δ 164.6, 160.1, 158.4, 157.7, 156.0, 154.4, 152.1, 149.2, 149.2, 145.8, 141.9, 127.8, 121.3, 121.3, 119.0, 115.5, 107.0, 97.6, 48.2, 41.9, 31.9, 31.0, 28.9, 28.9, 26.9, 26.7, 26.6, 24.6, 22.5, 22.0. HRMS (ESI) *m/z*: calcd for $C_{30}H_{36}N_6O$ $[M+H]^+$ 515.2930, found 515.2924.

3-Methyl-2-((7-((6-methyl-1,2,3,4-tetrahydroacridin-9-yl)amino)heptyl)amino)-6-(pyridin-4-yl)pyrimidin-4(3*H*)-one (**27e**). Yellow solid, 66% yield: Rf = 0.6 (10% methanol in dichloromethane). ^{1}H NMR (300 MHz, CD_3OD) δ 8.58 (d, *J* = 5.8 Hz, 2H), 8.21 (d, *J* = 8.9 Hz, 1H), 7.94 (d, *J* = 5.9 Hz, 2H), 7.51 (s, 1H), 7.38 (d, *J* = 9.0 Hz, 1H), 6.38 (s, 1H), 3.90 (t, *J* = 7.2 Hz, 2H), 3.61 (t, *J* = 7.0 Hz, 2H), 3.43 (s, 3H), 2.98 (s, 2H), 2.61 (d, *J* = 15.3 Hz, 2H), 2.55 (s, 3H), 1.96 (s, 4H), 1.81 (d, *J* = 24.7 Hz, 4H), 1.51 (m, 6H). ^{13}C NMR (75 MHz, CD_3OD) δ 164.6, 158.3, 156.2, 154.5, 149.5, 149.2, 149.2, 145.8, 144.3, 138.8, 127.0, 124.9, 121.2, 121.2, 118.1, 113.6, 110.9, 97.5, 47.9, 41.9, 30.3, 28.9, 28.8, 28.0, 27.1, 26.6, 26.5, 23.4, 21.8, 21.0, 20.6. HRMS (ESI) *m/z*: calcd for $C_{31}H_{39}N_6O$ $[M+H]^+$ 511.3180, found 511.3179.

2-((7-((6-Bromo-1,2,3,4-tetrahydroacridin-9-yl)amino)heptyl)amino)-6-(3-fluoropyridin-4-yl)-3-methylpyrimidin-4(3*H*)-one (**27f**). Yellow solid, 65% yield: Rf = 0.6 (10% methanol in dichloromethane). ^{1}H NMR (300 MHz, CD_3OD) δ 8.53 (s, 1H), 8.45 (d, *J* = 4.9 Hz, 1H), 8.32 - 8.20 (m, 1H), 8.05 (t, *J* = 5.8 Hz, 1H), 7.38 (d, *J* = 10.0 Hz, 1H), 7.25 (t, *J* = 8.5 Hz, 1H), 6.43 (s, 1H), 3.71 (t, *J* = 7.1 Hz, 2H), 3.55 (t, *J* = 7.1 Hz, 2H), 3.43 (s, 3H), 2.98 (s, 2H), 2.69 (s, 2H), 1.94 (s, 4H), 1.74 (s, 4H), 1.42 (m, 6H). ^{13}C NMR (75 MHz, CD_3OD) δ 164.3, 158.8, 156.7, 156.2, 154.2, 152.3, 145.3, 145.3, 138.7, 138.4, 133.2, 126.9, 125.4, 123.9, 123.7, 117.2, 114.5, 102.6, 48.6, 41.9,

31.7, 30.9, 28.9, 28.9, 27.0, 26.7, 26.6, 24.3, 22.4, 21.8. HRMS (ESI) *m/z*: calcd for $C_{30}H_{35}BrFN_6O$ $[M+H]^+$ 593.2035, found 593.2043.

2-((7-((6-Chloro-1,2,3,4-tetrahydroacridin-9-yl)amino)heptyl)amino)-6-(3-fluoropyridin-4-yl)-3-methylpyrimidin-4(3*H*)-one (**27g**). Yellow solid, 69% yield: Rf = 0.6 (10% methanol in dichloromethane). ^{1}H NMR (300 MHz, CD_3OD) δ 8.53 (s, 1H), 8.45 (d, *J* = 4.9 Hz, 1H), 8.32 - 8.22 (m, 1H), 8.05 (t, *J* = 5.8 Hz, 1H), 7.38 (d, *J* = 10.0 Hz, 1H), 7.25 (t, *J* = 8.5 Hz, 1H), 6.43 (s, 1H), 3.71 (t, *J* = 7.1 Hz, 2H), 3.55 (t, *J* = 7.1 Hz, 2H), 3.43 (s, 3H), 2.98 (s, 2H), 2.69 (s, 2H), 1.94 (s, 4H), 1.74 (s, 4H), 1.45 (m, 6H). ^{13}C NMR (75 MHz, CD_3OD) δ 164.3, 156.5, 154.2, 153.0, 145.3, 144.9, 138.7, 138.5, 135.7, 133.2, 125.5, 124.4, 123.9, 123.5, 116.8, 114.3, 102.6, 102.5, 48.6, 41.9, 31.6, 31.0, 28.9, 28.9, 27.1, 26.7, 26.6, 24.2, 22.3, 21.8. HRMS (ESI) *m/z*: calcd for $C_{30}H_{35}ClFN_6O$ $[M+H]^+$ 549.2540, found 549.2542.

2-((7-((6-Fluoro-1,2,3,4-tetrahydroacridin-9-yl)amino)heptyl)amino)-6-(3-fluoropyridin-4-yl)-3-methylpyrimidin-4(3*H*)-one (**27h**). Yellow solid, 69% yield: Rf = 0.5 (10% methanol in dichloromethane). ^{1}H NMR (300 MHz, CD_3OD) δ 8.53 (s, 1H), 8.45 (d, *J* = 4.9 Hz, 1H), 8.30 - 8.20 (m, 1H), 8.05 (t, *J* = 5.8 Hz, 1H), 7.38 (d, *J* = 10.0 Hz, 1H), 7.25 (t, *J* = 8.5 Hz, 1H), 6.43 (s, 1H), 3.71 (t, *J* = 7.1 Hz, 2H), 3.55 (t, *J* = 7.1 Hz, 2H), 3.43 (s, 3H), 2.98 (s, 2H), 2.69 (s, 2H), 1.94 (s, 4H), 1.74 (s, 4H), 1.45 (m, 6H). ^{13}C NMR (75 MHz, CD_3OD) δ 164.3, 162.2, 158.8, 156.2, 155.2, 154.2, 153.8, 145.3, 138.7, 133.2, 127.0, 123.9, 114.9, 114.0, 113.7, 113.2, 107.5, 102.6, 48.5, 41.9, 30.8, 30.8, 28.9, 28.9, 27.0, 26.7, 26.6, 24.0, 22.2, 21.5. HRMS (ESI) *m/z*: calcd for $C_{30}H_{35}F_2N_6O$ $[M+H]^+$ 533.2835, found 533.2841.

2-((7-((7-Fluoro-1,2,3,4-tetrahydroacridin-9-yl)amino)heptyl)amino)-6-(3-fluoropyridin-4-yl)-3-methylpyrimidin-4(3*H*)-one (**27i**). Brown solid, 61% yield: Rf = 0.5 (10% methanol in dichloromethane). ^{1}H NMR (300 MHz, CD_3OD) δ 8.52 (d, *J* = 3.1 Hz, 1H), 8.44 (d, *J* = 4.9 Hz, 1H), 8.04 (t, *J* = 5.9 Hz, 1H), 7.85 - 7.73 (m, 2H), 7.44 (t, *J* = 8.6 Hz, 1H), 6.42 (s, 1H), 3.55 (dd, *J* = 16.5, 7.7 Hz, 4H), 3.42 (s, 3H), 2.98 (s, 2H), 2.74 (s, 2H), 1.92 (s, 4H), 1.69 (s, 4H), 1.42 (m, 6H). ^{13}C NMR (75 MHz, CD_3OD) δ 164.3, 160.1, 158.8, 157.6, 156.2, 155.9, 154.2, 152.2, 145.3, 141.7, 138.7, 133.2, 127.7, 123.9, 119.3, 115.3, 107.4, 102.6, 48.3, 41.9, 31.8, 31.0, 28.9, 28.9, 27.0, 26.7, 26.6, 24.6, 22.5, 21.9. HRMS (ESI) *m/z*: calcd for $C_{30}H_{35}F_2N_6O$ $[M+H]^+$ 533.2835, found 533.2843.

6-(3-Fluoropyridin-4-yl)-3-methyl-2-((7-((1,2,3,4-tetrahydroacridin-9-yl)amino)heptyl)amino)pyrimidin-4(3*H*)-one (**27j**). Yellow solid, 61% yield: Rf = 0.5 (10%

methanol in dichloromethane). ^{1}H NMR (300 MHz, CD_3OD) δ 8.52 (d, J = 3.1 Hz, 1H), 8.45 (d, J = 4.8 Hz, 1H), 8.25 (d, J = 8.7 Hz, 1H), 8.05 (t, J = 5.9 Hz, 1H), 7.80 - 7.67 (m, 2H), 7.49 (d, J = 5.9 Hz, 1H), 6.42 (s, 1H), 3.78 (t, J = 7.0 Hz, 2H), 3.56 (t, J = 7.0 Hz, 2H), 3.43 (s, 3H), 3.01 (s, 2H), 2.71 (s, 2H), 1.95 (s, 4H), 1.84 - 1.63 (m, 4H), 1.46 (m, 6H). ^{13}C NMR (75 MHz, CD_3OD) δ 164.3, 158.8, 156.2, 154.7, 154.2, 152.9, 145.3, 141.5, 138.7, 133.2, 131.2, 124.5, 124.3, 123.8, 121.9, 117.2, 112.9, 102.5, 48.3, 41.9, 30.7, 29.9, 28.9, 28.8, 27.1, 26.6, 26.6, 24.0, 22.1, 21.2. HRMS (ESI) *m/z*: calcd for $C_{30}H_{36}FN_6O$ $[M+H]^+$ 515.2930, found 515.2937.

6-(3-Fluoropyridin-4-yl)-3-methyl-2-((7-((6-methyl-1,2,3,4-tetrahydroacridin-9-yl)amino)heptyl)amino)pyrimidin-4(3*H*)-one (**27k**). Yellow solid, 61% yield: Rf = 0.6 (10% methanol in dichloromethane). ^{1}H NMR (300 MHz, CD_3OD) δ 8.50 (d, J = 3.2 Hz, 1H), 8.43 (d, J = 4.8 Hz, 1H), 8.21 (d, J = 8.9 Hz, 1H), 8.05 (t, J = 5.9 Hz, 1H), 7.52 (s, 1H), 7.38 (d, J = 8.9 Hz, 1H), 6.39 (s, 1H), 3.90 (t, J = 7.3 Hz, 2H), 3.58 (t, J = 7.0 Hz, 2H), 3.44 (s, 3H), 3.00 (s, 2H), 2.62 (d, J = 16.0 Hz, 2H), 2.56 (s, 3H), 1.97 (s, 4H), 1.80 (d, J = 26.0 Hz, 4H), 1.50 (m, 6H). ^{13}C NMR (75 MHz, CD_3OD) δ 164.3, 158.8, 156.2, 154.2, 149.6, 145.3, 144.2, 138.9, 138.7, 138.4, 133.1, 127.1, 124.8, 123.9, 118.2, 113.7, 111.0, 102.5, 47.9, 41.9, 30.4, 28.9, 28.8, 28.1, 27.2, 26.6, 26.5, 23.4, 21.8, 21.0, 20.6. HRMS (ESI) *m/z*: calcd for $C_{31}H_{38}FN_6O$ $[M+H]^+$ 529.3086, found 529.3096.

Pharmacology

AChE Activity Assay In Vitro. The *in vitro* inhibitory assay against AChE was performed using Ellman's method with modification.[57] The cerebral cortex of mouse was homogenized in cold 75 mM sodium phosphate buffer (pH = 7.4) with 0.4 mM tetraisopropylpyrophosphoramide as the AChE source. The reaction was initiated by a mixture of 1 μL of test compounds (40 μM final concentration for primary screening) or solvent, 50 μL of 0.1 M phosphate buffer, 50 μL of 0.2% dithionitrobenzoic acid (Sigma), 109 μL of deionized water, 10 μL of mouse cortex homogenate, and 30 μL of 2 mM acetylthiocholine iodide (Sigma) as the substrate of the AChE enzymatic reaction, and then incubated for 20 min at room temperature. The reaction was terminated by adding 50 μL of 3% sodium-dodecyl sulphate (SDS). The production of the yellow anion of 5-thio-2-nitrobenzoic acid was measured with a microplate reader at 450 nm. The inhibitory rates of tested compounds were normalized by AChE activity of the control group, and the IC_{50} was defined as the concentration of the compound that reduced 50% of the enzymatic activity without inhibitor.

GSK-3β Activity Assay In Vitro. The *in vitro* inhibitory effects of compounds on GSK-3*β* activity were evaluated with human recombinant GSK-3*β* (gifted from Prof. Yechun Xu from Shanghai Institute of Materia Medica, Chinese Academy of Sciences) by using Kinase-Glo reagent kit (Promega, Madison, WI, USA) according to previous method[58] with modification. Test compounds were dissolved and diluted with DMSO. The primary screening and IC_{50} evaluation were carried out in 96-well black plate. The reaction was initiated by a mixture of 1 μL of test compounds at different concentrations (10 μM final concentration for the first-round compounds, 1 μM final concentration for the second-round compounds at primary screening), 10 μL (20 ng) of GSK-3*β* enzyme, and 89 μL of assay buffer containing substrate (25 μM final concentration) and adenosine triphosphate (ATP, 5 μM final concentration). After a 30 min incubation at 30 ^{o}C, the enzymatic reaction was terminated by adding 100 μL of Kinase-Glo reagent. Luminescence was recorded after 10 min using a microplate reader. The inhibitory rates of tested compounds were normalized by GSK-3*β* activity of the control group, and the IC_{50} was defined as the concentration of the compound that reduced 50% of the enzymatic activity without inhibitor.

Molecular modeling. In our study, the protein structure of AChE was derived from the complex of recombinant human AChE and donepezil (**1**),[59] downloaded from the Protein Data Bank (PDB code: 4EY7). And the protein structure of GSK-3*β* was derived from the complex of GSK-3*β* and an oxadiazole derivative,[60] downloaded from the Protein Data Bank (PDB code: 3F88). The preprocessing of two proteins was conducted using Protein Preparation Wizard, and Compounds **23e** and **27g** were prepared using LigPrep, both in Schrodinger software. The molecular docking between enzymes and compounds was performed by employing the Schrodinger Glide procedure, respectively. Subsequently, the docking results were disposed as figures using PyMOL software.

BBB assay. UPLC-MS/MS system was employed to detect the concentration of compound **27g** in the brain and plasma. The experimental protocols were evaluated and approved by the Ethics Committee of the China Pharmaceutical University (IACUC NO. 2020-06-004). Adult female ICR mice were purchased from the Qinglongshan Animal Breeding Ground (Nanjing, China). Compound **27g** was dissolved in PBS containing 10% DMSO and 20% (2-hydroxypropyl)-*β*-

cyclodextrin. Instrumentation system included ACQUITY UPLC I-Class Plus chromatograph, Xevo TQ-XS mass spectrometer, and MassLynx V4.2 operational software. Animals were divided into four groups (n=4 in each group) and treated with **27g** at a dosage of 15 mg/kg (i.p.). After the administration for 0.5 h, 1 h, 2 h, and 4 h, mice were executed by drawing blood from femoral artery (about 300 μL). Brain tissues were immediately taken out and washed with normal saline. All samples after centrifugation for 5 min (8000 rpm) were detected for the concentration of **27g** using UPLC-MS/MS system.

Pharmacokinetic properties investigation. UPLC-MS/MS system was also employed to detect the concentration of compound **27g** in plasma. The experimental protocols were evaluated and approved by the Ethics Committee of the China Pharmaceutical University (IACUC NO. 2020-06-004). Adult female ICR mice were purchased from the Qinglongshan Animal Breeding Ground (Nanjing, China). Compound **27g** was dissolved in PBS containing 10% DMSO and 20% (2-hydroxypropyl)-β-cyclodextrin, and the mixed solution of DMSO/PEG300/normal saline (5:45:50, v/v/v) was used for i.v. injection. Instrumentation system included ACQUITY UPLC I-Class Plus chromatograph, Xevo TQ-XS mass spectrometer, and MassLynx V4.2 operational software. Animals were divided into two groups (n=3 in each group) and administered with compound **27g** by i.p. (15 mg/kg) or i.v. (5 mg/kg). After the administration for 2 min, 5 min, 0.25 h, 0.5 h, 1 h, 2 h, 4 h, 8 h, 12 h, and 24 h, heparinized blood (about 50 μL for each mouse) was collected from orbital venous plexus to anticoagulant tubes. Subsequently, the centrifugation of the above blood afforded serum samples (8000 rpm for 5 min) which were tested for the concentration of **27g** using UPLC-MS/MS system. And related pharmacokinetic parameters of **27g** were calculated using WinNonlin version 6.4 software.

Behavioral studies. The experimental protocols were evaluated and approved by the Ethics Committee of the China Pharmaceutical University (IACUC NO. 20201111135). Behavioral studies were performed with adult female ICR mice (8-10 weeks old, weight 25-30 g), which were purchased from the Zhejiang Academy of Medical Sciences (Hangzhou, China). Scopolamine hydrobromide and tacrine were supplied by Aladdin Reagents (Shanghai, China). The test agents were prepared in a blank solution which was PBS containing 10% DMSO and 20% (2-

hydroxypropyl)-β-cyclodextrin.

The mice were divided into five groups and compounds were given to each group as follows: (i) vehicle, (ii) scopolamine, (iii) tacrine plus scopolaminel, (iv) compound **23e** plus scopolamine, and (v) compound **27g** plus scopolamine. In the first period (d 1-10), scopolamine (15 mg/kg) was administered to groups (iii), (iv), and (v). In the second period (d 11-25), after the i.p. injection of scopolamine (15 mg/kg) for 30 min, tacrine (15 mg/kg), **23e** (15 mg/kg), and **27g** (15 mg/kg) were i.p. injected to mice in groups (iii), (iv), and (v), respectively. In the entire period (d 1-25), the blank solution was treated to group (i) each day and scopolamine (15 mg/kg) was administered to group (ii) each day.

Cognitive function was evaluated by the ANY-maze Video Tracking System. MWM was placed in a well-lit room and the opaque circular pool (120 cm diameter, 60 cm height) was filled with water (40 cm in depth) and sustained at 25 ℃. The maze was divided into four equal quadrants, and an escape platform (10 cm diameter) was located in the center of the fourth quadrant of the maze, labeled by a small flag (5 cm tall). The behavioral studies of each mouse included four consecutive d of learning and memory training (d 21-24) and three d of cognitive evaluation (d 23-25). The animal starting positions, facing the pool wall, were pseudorandomized for each trial. During the d 21-24, mice were trained once to find the platform in each quadrant for one trial (four times in total for each mouse). If an animal failed to find the platform within 120 s, the test ended and the animal was gently navigated to the platform by hand. Whether a mouse found or failed to find the platform within 120 s, it was kept on the platform for 10 s. For the cognitive evaluation, each mouse was individually evaluated on both visible-platform (d 23-24) and hidden-platform (day 25) versions of the water maze. In d 23-24, the latency and distance taken for mouse to reach the platform (a successful escape) from the second quadrant was recorded. On day 25, the platform was removed and the animals were given a probe trial in which mice had 120 s to search for the platform. The time taken to reach the missing platform and the number of times that animals crossed the missing platform location were recorded.

Data for the escape latency (latency to the first entry), the distances traveled (distance to the first entry), and the number of platform location crossings (entering times) were recorded by ANY-maze Video Tracking System and processed by GraphPad Prism 8.

Differentiation of SH-SY5Y cells. SH-SY5Y neuroblastoma cells were differentiated into corresponding neurons using the method described by Shipley and co-workers[61] with some modifications. Briefly, SH-SY5Y cells were plated with Basic Growth Media and allowed to reach 70% confluency. Subsequently, media was changed to Differentiation Media #1 and replaced every 48 h for the following 7 d. Cells were then split 1:1 and moved into fresh flasks and Differentiation Media #2 was added. Then, Differentiation Media #2 was replaced every 48 h for the following 4 d. Subsequently, media was changed with Differentiation Media #3 and replaced every 48 h for the following 7 d. After this period, SH-SY5Y derived neurons could be acquired and used for subsequent assays and analysis. The specific ingredients of each media were shown as follows (the full name of the corresponding ingredient could be found in the Abbreviations Section).

Basic Growth Media	Differentiation Media #1	Differentiation Media #2	Differentiation Media #3
EMEM	EMEM	EMEM	Neurobasal
15% hiFBS	2.5% hiFBS	1% hiFBS	20 mM KCl
1 x Pen/Strep	1 x Pen/Strep	1 x Pen/Strep	1 x Pen/Strep
2 mM Glutamine	2 mM Glutamine	2 mM Glutamine	2 mM Glutamine
	10 μM RA	10 μM RA	10 μM RA
			50 ng/mL BDNF

Measurements of p-Tau and total tau protein levels. SH-SY5Y cells were cultured on different types of media and differentiated to SH-SY5Y neurons as described above. Then, SH-SY5Y derived neurons were treated with 0.7 mM GA for 24 h as described by Takeuchi group.[62] Compounds to be tested were co-incubated with GA for 24 h at appropriate concentrations. Levels of total tau and p-Tau were measured as follows. A total of 3×10^5 cells were lysed using 100 μL Cell Extraction Buffer (Thermo Fisher), followed by incubation for 20 min on ice. Cells lysate were subsequently centrifuged at the force of 14000 $\times$ g for 15 min, supernatants were used for subsequent analysis. Phosphorylation levels of tau protein on S199 and S396 were quantified using the methodology of enzyme-linked immunosorbent assay (ELISA). ELISA kit KHB7041 (Thermo Fisher) was used to quantify p-Tau on S199 site following the manufacturer recommended protocol. ELISA kit

KHB7031 (Thermo Fisher) was used to quantify p-Tau on S396 site following the manufacturer recommended protocol. ELISA kit KHB0041 (Thermo Fisher) was used to quantify total tau protein following the manufacturer's recommended protocol. Phosphorylation percentage was obtained for the analyzed residues, by normalization against total Tau.

Cell viability assay of SH-SY5Y derived neurons. A total of 10^5 cells per well were seeded into a 96-well plate. After SH-SY5Y differentiation by the continuous treatment of RA,[61] cells were treated with 0.7 mM GA. Along with GA treatment, an appropriate concentration of test compounds was added. After 24 h, 25 μL of 5 mg/mL Thiazolyl blue (MTT) (Sigma) were added into each well without removing cell culture media and incubated at 37 ^{o}C with 5% CO_2 for 2 h. Subsequently, 100 μL of lysing buffer (50% SDS solution, 25% DMF, 25% demineralized water) was added. After overnight incubation (20 h) at 37 ^{o}C, the optical densities at 490 nm were measured using a microplate reader. The medium/MTT/lysing buffer incubated under the same conditions was used as the control.

Morphology studies in neuronal system. Cells were fixed in 4% paraformaldehyde (PFA) for 20 min at room temperature. Samples were then washed three times using 1% PBS in Tween-20 (PBS-T) for 2 min, and subsequently placed in 5% normal goat serum (NGS) in PBS-T (NGS-T) for 2 h at room temperature. After removing the 5% NGS-T, the mouse anti-β tubulin primary antibody was added at a final concentration of 1:1000 and left to incubate overnight at 4 ^{o}C. The primary antibody was then washed with 1% PBS-T three times, and subsequently the rabbit anti-mouse secondary antibody was added at a final 1:1200 concentration. The sample was allowed to incubate for 1 h at room temperature and subsequently mounted for confocal imaging. Cells images were acquired using Zeiss880 Confocal Microscope. Laser power was set at 4%, gained 650, and digital offset at 350. Acquisition speed was set at 1.3 m averaging 2 times per image. Morphological analysis of SH-SY5Y derived neurons confocal images was performed using the ImageJ software with the NeuronJ plug-in.

ASSOCIATED CONTENT

Supporting Information

The Supporting Information is available free of charge on the ACS Publications website at DOI:

Experimental methods for biological assays; figures, tables, NMR spectra, HPLC spectra, MS spectra (PDF)

Molecular formula strings and some data (CSV)

AUTHOR INFORMATION

Corresponding Authors

*E-mail: hzhang@simm.ac.cn (for H.Z.)

*E-mail: Zheying.Zhu@nottingham.ac.uk (for Z.Z.)

*E-mail: jinyixu@china.com (for J.X.)

Author Contributions

#H.Y., G.U., and P.Z. contributed equally to this work.

Notes

The authors declare no competing financial interest. Qi Gong and Ying Yin performed the assays of enzymatic inhibitory activities of AChE and GSK-3β under the instruction of Haiyan Zhang, and Renren Bai performed the behavioral studies of mice using the MWM test.

ACKNOWLEDGMENTS

This study was supported from the National Natural Science Foundation of China (nos. 81874289 and 81903446), The Open Project of State Key Laboratory of Natural Medicines, China Pharmaceutical University (SKLNMKF 201710), the Natural Science Foundation of Jiangsu Province (BK20190564), the China Postdoctoral Science Foundation Grant 2019M652037, and "Double First-Class" University project (nos. CPU2018GY04, CPU2018GY35), China Pharmaceutical University. This study was also funded by School of Pharmacy, The University of Nottingham (RJ/T5433).

ABBREVIATIONS

A*β*, *β*-amyloid; ACh, acetylcholine; AChE, acetylcholinesterase; AChEIs, AChE inhibitors; AD, Alzheimer's disease; ATP, adenosine triphosphate; AUC, area under curve; BACE-1, *β*-site amyloid precursor protein cleaving enzyme; BBB, blood-brain barrier; BDNF, brain derived neurotrofic factor; CAS, catalytic anionic site; CDI, *N*,*N'*-carbonyldiimidazole; CL, clearance rate; CMC-Na, sodium carboxymethyl cellulose; DMSO, dimethyl sulfoxide; ELISA, enzyme linked immunosorbent assay; EMEM, Eagle's minimum essential medium; GA, glyceraldehyde; GSK-3*β*, glycogen synthase kinase 3 beta; HFIP, hexafluoroisopropanol; hiFBS, heat-inactivated fetal bovine serum; HPLC, high-performance liquid chromatography; HRMS high-resolution mass spectrometry; i.p., intraperitoneal; i.v., intravenous; MRT, mean residence time; MTT, Thiazolyl blue; MWM, Morris water maze; NCEs, new chemical entities; NFTs, neurofibrillary tangles; NGS, normal goat serum; NGS-T, NGS in PBS-T; NMDA, *N*-methyl-D-aspartate; PAS, peripheral anionic site; PBS, phosphate buffer saline; PBS-T, PBS in Tween-20; Pen/Strep, penicillin-streptomycin solution; PFA, paraformaldehyde; p.o., oral administration; p-Tau, phosphorylated tau protein; RA, retinoic acid; S199, serine-199; S396, serine-396; SARs, structure-activity relationships; SDS, sodium-dodecyl sulphate; SP, senile plaques; THF, tetrahydrofuran; ThT, Thioflavine-T; TLC, thin-layer chromatography.

REFERENCES

(1) Hung, S. Y.; Fu, W. M. Drug candidates in clinical trials for Alzheimer's disease. *J. Biomed. Sci.* **2017**, *24*, 47.

(2) Ulep, M. G.; Saraon, S. K.; McLea, S. Alzheimer disease. *J. Nurse Pract.* **2018**, *14*, 129-135.

(3) Blennow, K.; de Leon, M. J.; Zetterberg, H. Alzheimer's disease. *Lancet* **2006**, *368*, 387-403.

(4) Alzheimer, A. Uber eine eigenartige Erkrankung der Hirnrinde, *Allg. Z. Psychiatr.* **1907**, *64*, 146-148.

(5) Ferreira-Vieira, T. H.; Guimaraes, I. M.; Silva, F. R.; Ribeiro, F. M. Alzheimer's disease: targeting the cholinergic system. *Curr. Neuropharmacol.* **2016**, *14*, 101-115.

(6) Panza, F.; Solfrizzi, V.; Seripa, D.; Imbimbo, B. P.; Lozupone, M.; Santamato, A.; Zecca, C.; Barulli, M. R.; Bellomo, A.; Pilotto, A.; Daniele, A.; Greco, A.; Logroscino, G. Tau-centric targets and drugs in clinical development for the treatment of Alzheimer's disease. *Biomed. Res. Int.* **2016**,

2016, 3245935.

(7) Hardy, J.; Selkoe, D. J. The amyloid hypothesis of Alzheimer's disease: progress and problems on the road to therapeutics. *Science* **2002**, *297*, 353-356.

(8) Youdim, M. B. H.; Bakhle, Y. S. Monoamine oxidase: isoforms and inhibitors in Parkinson's disease and depressive illness. *Brit. J. Pharmacol.* **2006**, *147*, S287-S296.

(9) Kepp, K. P. Bioinorganic chemistry of Alzheimer's disease. *Chem. Rev.* **2012**, *112*, 5193-5239.

(10) Shimizu, E.; Tang, Y. P.; Rampon, C.; Tsien, J. Z. NMDA receptor-dependent synaptic reinforcement as a crucial process for memory consolidation. *Science* **2000**, *290*, 1170-1174.

(11) Rodriguez, J. J.; Noristani, H. N.; Verkhratsky, A. The serotonergic system in ageing and Alzheimer's disease. *Prog. Neurobiol.* **2012**, *99*, 15-41.

(12) Panula, P.; Chazot, P. L.; Cowart, M.; Gutzmer, R.; Leurs, R.; Liu, W. L. S.; Stark, H.; Thurmond, R. L.; Haas, H. L. International union of basic and clinical pharmacology. XCVIII. Histamine receptors. *Pharmacol. Rev.* **2015**, *67*, 601-655.

(13) Heckman, P. R. A.; Wouters, C.; Prickaerts, J. Phosphodiesterase inhibitors as a target for cognition enhancement in aging and Alzheimer's disease: a translational overview. *Curr. Pharm. Design* **2015**, *21*, 317-331.

(14) Zhang, P.; Xu. S.; Zhu. Z.; Xu. J. Multi-target design strategies for the improved treatment of Alzheimer's disease. *Eur. J. Med. Chem.* **2019**, *176*, 228-247.

(15) Zemek, F.; Drtinova, L.; Nepovimova, E.; Sepsova, V.; Korabecny, J.; Klimes, J.; Kuca, K. Outcomes of Alzheimer's disease therapy with acetylcholinesterase inhibitors and memantine. *Expert. Opin. Drug Saf.* **2014**, *13*, 759-774.

(16) Cavalli, A.; Bolognesi, M. L.; Minarini, A.; Rosini, M.; Tumiatti, V.; Recanatini, M.; Melchiorre. C. Multi-target-Directed Ligands To Combat Neurodegenerative Diseases. *J. Med. Chem*. **2008**, *51*, 347–372.

(17) Davies. P.; Maloney. A. J. Selective loss of central cholinergic neurons in Alzheimer's disease, *Lancet* **1976**, *308*, 1403-1403.

(18) Bartus, R. T.; Dean, R. L.; Beer, B.; Lippa, A. S. The cholinergic hypothesis of geriatric memory dysfunction. *Science* **1982**, *217*, 408-414.

(19) Augustinsson. K. B.; Nachmansohn. D. Distinction between acetylcholine-esterase and other choline ester-splitting enzymes, *Science* **1949**, *110*, 98-99.

(20) Kumar, A.; Singh, A.; Ekavali. A review on Alzheimer's disease pathophysiology and its management: an update. *Pharmacol. Rep.* **2015**, *67*, 195-203.

(21) Bartolini, M.; Bertucci, C.; Cavrini, V.; Andrisano, V. Beta-amyloid aggregation induced by human acetylcholinesterase: inhibition studies. *Biochem. Pharmacol.* **2003**, *65*, 407-416.

(22) Castro, A.; Martinez, A. Targeting beta-amyloid pathogenesis through acetylcholinesterase inhibitors. *Curr. Pharm. Des.* **2006**, *12*, 4377-4387.

(23) Liu, F.; Liang, Z. H.; Shi, J. H.; Yin, D. M.; El-Akkad, E.; Grundke-Iqbal, I.; Iqbal, K.; Gong, C. X. PKA modulates GSK-3 beta- and cdk5-catalyzed phosphorylation of tau in site- and kinase-specific manners. *FEBS Lett.* **2006**, *580*, 6269-6274.

(24) Iba, M.; Guo, J. L.; McBride, J. D.; Zhang, B.; Trojanowski, J. Q.; Lee, V. M. Y. Synthetic tau fibrils mediate transmission of neurofibrillary tangles in a transgenic mouse model of Alzheimer's-like tauopathy. *J. Neurosci.* **2013**, *33*, 1024-1037.

(25) Maqbool, M.; Mobashir, M.; Hoda, N. Pivotal role of glycogen synthase kinase-3: a therapeutic target for Alzheimer's disease. *Eur. J. Med. Chem.* **2016**, *107*, 63-81.

(26) Phiel, C. J.; Wilson, C. A.; Lee, V. M. Y.; Klein, P. S. GSK-3 alpha regulates production of Alzheimer's disease amyloid-beta peptides. *Nature* **2003**, *423*, 435-439.

(27) Noh, M. Y.; Koh, S. H.; Kim, Y.; Kim, H. Y.; Cho, G. W.; Kim, S. H. Neuroprotective effects of donepezil through inhibition of GSK-3 activity in amyloid-beta-induced neuronal cell death. *J. Neurochem.* **2009**, *108*, 1116-1125.

(28) Yoshiyama, Y.; Kojima, A.; Ishikawa, C.; Arai, K. Anti-inflammatory action of donepezil ameliorates tau pathology, synaptic Loss, and neurodegeneration in a tauopathy mouse model. *J. Alzheimers Dis.* **2010**, *22*, 295-306.

(29) Garc á-Ayllon. M.; Small. D. H.; Avila. J.; Saez-Valero. J. Revisiting the role of acetylcholinesterase in Alzheimer's disease: cross-talk with p-Tau and *β*-amyloid. *Front. Mol. Neurosci.* **2011**, *4*, 1-9.

(30) Jiang, X. Y.; Chen, T. K.; Zhou, J. T.; He, S. Y.; Yang, H. Y.; Chen, Y.; Qu, W.; Feng, F.; Sun, H. P. Dual GSK-3 beta/AChE inhibitors as a new strategy for multitargeting anti-Alzheimer's disease drug discovery. *ACS Med. Chem. Lett.* **2018**, *9*, 171-176.

(31) Oukoloff, K.; Coquelle, N.; Bartolini, M.; Naldi, M.; Le Guevel, R.; Bach, S.; Josselin, B.; Ruchaud, S.; Catto, M.; Pisani, L.; Denora, N.; Lacobazzi, R. M.; Silman, I.; Sussman, J. L.; Buron,

F.; Colletier, J. P.; Jean, L.; Routier, S.; Renard, P. Y. Design, biological evaluation and X-ray crystallography of nanomolar multifunctional ligands targeting simultaneously acetylcholinesterase and glycogen synthase kinase-3. *Eur. J. Med. Chem.* **2019**, *168*, 58-77.

(32) Jiang, X. Y.; Zhou, J.T.; Wang, Y.; Chen, L.; Duan, Y.; Huang, J.P.; Liu, C.; Chen, Y.; Liu, W.Y.; Sun, H.P.; Feng, F.; Qu, W. Rational design and biological evaluation of a new class of thiazolopyridyl tetrahydroacridines as cholinesterase and GSK-3 dual inhibitors for Alzheimer's disease. *Eur. J. Med. Chem.* **2020**, *207*, 112751-112766.

(33) Ismaili, L.; Refouvelet, B.; Benchekroun, M.; Brogi, S.; Brindisi, M.; Gemma, S.; Campiani, G.; Filipic, S.; Agbaba, D.; Esteban, G.; Unzeta, M.; Nikolic, K.; Butini, S.; Marco-Contelles, J. Multitarget compounds bearing tacrine- and donepezil-like structural and functional motifs for the potential treatment of Alzheimer's disease. *Prog. Neurobiol.* **2017**, *151*, 4-34.

(34) Fernández-Bachiller, M. I.; Pérez, C.; González-Muñoz, G. C.; Conde, S.; López, M. G.; Villarroya, M.; Garc á, A. G.; Rodr guez-Franco, M. I. Novel tacrine-8-hydroxyquinoline hybrids as multifunctional agents for the treatment of Alzheimer's disease, with neuroprotective, cholinergic, antioxidant, and copper-complexing properties. *J. Med. Chem.* **2010**, *53*, 4927-4937.

(35) Zha, X.; Lamba, D.; Zhang, L.; Lou, Y.; Xu, C.; Kang, D.; Chen, L.; Xu, Y.; Zhang, L.; Simone, A. D.; Samez, S.; Pesaresi, A.; Stojan, J.; Lopez, M. G.; Egea, J.; Andrisano, V.; Bartolini, M. Novel tacrine-benzofuran hybrids as potent multitarget-directed ligands for the treatment of Alzheimer's disease: design, synthesis, biological evaluation, and X-ray crystallography. *J. Med. Chem.* **2016**, *59*, 114-131.

(36) Perez-Areales, F. J.; Garrido, M.; Aso E; Bartolini, M.; Simone, A. D.; Espargaro, A.; Ginex, T.; Sabate, R.; Perez, B.; Andrisano, V.; Puigoriol-Illamola, D.; Pallas, M.; Luque, F. J.; Loza, M. I.; Brea, J.; Ferrer, I.; Ciruela, F.; Messeguer, A.; Munoz-Torrero, D. Centrally active multitarget anti-Alzheimer agents derived from the antioxidant lead CR-6. *J. Med. Chem.* **2020**, *63*, 9360-9390.

(37) Uehara, F.; Shoda, A.; Aritomo, K.; Fukunaga, K.; Watanabe, K.; Ando, R.; Shinoda, M.; Ueno, H.; Kubodera, H.; Sunada, S.; Saito, K. I.; Kaji, T.; Asano, S.; Eguchi, J.; Yuki, S.; Tanaka, S.; Yoneyama, Y.; Niwa, T. 6-(4-Pyridyl)pyrimidin-4(3H)-ones as CNS penetrant glycogen synthase kinase-3 beta inhibitors. *Bioorg. Med. Chem. Lett.* **2013**, *23*, 6928-6932.

(38) Fukunaga, K.; Uehara, F.; Aritomo, K.; Shoda, A.; Hiki, S.; Okuyama, M.; Usui, Y.; Watanabe, K.; Yamakoshi, K.; Kohara, T.; Hanano, T.; Tanaka, H.; Tsuchiya, S.; Sunada, S.; Saito,

K. I.; Eguchi, J.; Yuki, S.; Asano, S.; Tanaka, S.; Mori, A.; Yamagami, K.; Baba, H.; Horikawa, T.; Fujimura, M. 2-(2-Phenylmorpholin-4-yl)pyrimidin-4(3H)-ones; a new class of potent, selective and orally active glycogen synthase kinase-3 beta inhibitors. *Bioorg. Med. Chem. Lett.* **2013**, *23*, 6933-6937.

(39) Mistry, P. T.; Kamdar, N. R.; Haveliwala, D. D.; Patel, S. K. Synthesis, characterization, and in vitro biological studies of some novel pyran fused pyrimidone derivatives. *J. Heterocyclic Chem.* **2012**, *49*, 349-357.

(40) Fukunaga, K.; Sakai, D.; Watanabe, K.; Nakayama, K.; Kohara, T.; Tanaka, H.; Sunada, S.; Nabeno, M.; Okamoto, M.; Saito, K.; Eguchi, J.; Mori, A.; Tanaka, S.; Inazawa, K.; Horikawa, T. Discovery of novel 2-(alkylmorpholin-4-yl)-6-(3-fluoropyridin-4-yl)pyrimidin-4(3H)-ones as orally-active GSK-3 beta inhibitors for Alzheimer's disease. *Bioorg. Med. Chem. Lett.* **2015**, *25*, 1086-1091.

(41) Bhat, R.; Xue, Y. F.; Berg, S.; Hellberg, S.; Ormo, M.; Nilsson, Y.; Radesater, A. C.; Jerning, E.; Markgren, P. O.; Borgegard, T.; Nylof, M.; Gimenez-Cassina, A.; Hernandez, F.; Lucas, J. J.; Diaz-Nido, J.; Avila, J. Structural insights and biological effects of glycogen synthase kinase 3-specific inhibitor AR-A014418. *J. Biol. Chem.* **2003**, *278*, 45937-45945.

(42) Han, Y. F.; Tang , X. C. Pharmacological profile of Huperzine A, a novel acetylcholinesterase inhibitor from Chinese herb. CNS Drug Rev. **1999**, *5*, 281-300.

(43) Liu, J.; Zhang, H. Y., Wang, L.M.; Tang, X.C. Inhibitory effects of huperzine B on cholinesterase activity in mice. Acta Pharmacol. Sin. **1999**, *20*,141-145.

(44) Wilcken, R.; Zimmermann, M. O.; Lange, A.; Joerger, A. C.; Boeckler, F. M. Principles and applications of halogen bonding in medicinal chemistry and chemical biology. *J. Med. Chem.* **2013**, *56*, 1363-1388.(45) Shipley, M. M.; Mangold, C. A.; Szpara, M. L. Differentiation of the SH-SY5Y human neuroblastoma cell line. *J. Vis. Exp.* **2016**, *108*, e53193.

(46) Koriyama, Y.; Furukawa, A.; Muramatsu, M.; Takino, J.; Takeuchi, M. Glyceraldehyde caused Alzheimer's disease-like alterations in diagnostic marker levels in SH-SY5Y human neuroblastoma cells. *Sci. Rep.* **2015**, *5*, 13313.

(47) Fu, Z. Q.; Yang, Y.; Song, J.; Jiang, Q. A.; Liu, Z. C.; Wang, Q.; Zhu, L. Q.; Wang, J. Z.; Tian, Q. LiCl attenuates thapsigargin-induced tau hyperphosphorylation by inhibiting GSK-3 beta in vivo and in vitro. *J. Alzheimers Dis.* **2010**, *21*, 1107-1117.

(48) Lovestone, S.; Boada, M.; Dubois, B.; Hull, M.; Rinne, J. O.; Huppertz, H. J.; Calero, M.; Andres, M. V.; Gomez-Carrillo, B.; Leon, T.; del Ser, T.; Investigators, A. A phase II trial of tideglusib in Alzheimer's disease. *J. Alzheimers Dis.* **2015**, *45*, 75-88.

(49) Wakasaya, Y.; Kawarabayashi, T.; Watanabe, M.; Yamamoto-Watanabe, Y.; Takamura, A.; Kurata, T.; Murakami, T.; Abe, K.; Yamada, K.; Wakabayashi, K.; Sasaki, A.; Westaway, D.; Hyslop, P. S. G.; Matsubara, E.; Shoji, M. Factors responsible for neurofibrillary tangles and neuronal cell losses in tauopathy. *J. Neurosci. Res.* **2011**, *89*, 576-584.

(50) Sorrells, S. F.; Paredes, M. F.; Ebrian-Silla, A. C.; Sandoval, K.; Qi, D. S.; Kelley, K. W.; James, D.; Mayer, S.; Chang, J.; Auguste, K. I.; Hang, E. F. C.; Gutierrez, A. J.; Kriegstein, A. R.; Mathern, G. W.; Oldham, M. C.; Huang, E. J.; Garcia-Verdugo, J. M.; Yang, Z. G.; Alvarez-Buylla, A. Human hippocampal neurogenesis drops sharply in children to undetectable levels in adults. *Nature* **2018**, *555*, 377-381.

(51) Head, B. P.; Patel, H. H.; Insel, P. A. Interaction of membrane/lipid rafts with the cytoskeleton: impact on signaling and function: membrane/lipid rafts, mediators of cytoskeletal arrangement and cell signaling. *Biochim. Biophys. Acta* **2014**, *1838*, 532-545.

(52) Hughes, J. P.; Rees, S.; Kalindjian, S. B.; Philpott, K. L. Principles of early drug discovery. *Brit. J. Pharmacol.* **2011**, *162*, 1239-1249.

(53) Abbott, N. J.; Patabendige, A. A. K.; Dolman, D. E. M.; Yusof, S. R.; Begley, D. J. Structure and function of the blood-brain barrier. *Neurobiol. Dis.* **2010**, *37*, 13-25.

(54) Morris, R. Developments of a water-maze procedure for the studying spatial learning in the rat. *J. Neurosci. Methods* **1984**, *11*, 47-60.

(55) Chen, Y.; Lin, H.; Zhu, J.; Gu, K.; Li, Q.; He, S.; Lu, X.; Tan, R.; Pei, Y.; Wu, L.; Bian, Y.; Sun, H. Design, synthesis, in vitro and in vivo evaluation of tacrine-cinnamic acid hybrids as multi-target acetyl-and butyrylcholinesterase inhibitors against Alzheimer's disease, *RSC Adv.* **2017**, *7*, 33851-33867.

(56) Zhang, C. J.; Yang, K.; Yu, S. H.; Su, J.; Yuan, S. L.; Han, J. X.; Chen, Y.; Gu, J. P.; Zhou, T.; Bai, R. R.; Xie, Y. Y. Design, synthesis and biological evaluation of hydroxypyridinone-coumarin hybrids as multimodal monoamine oxidase B inhibitors and iron chelates against Alzheimer's disease. *Eur. J. Med. Chem.* **2019**, *180*, 367-382.

(57) Ellman, G. L.; Courtney, K. D.; Andres, V., Jr.; Featherstone, R. M. A new and rapid

colorimetric determination of acetylcholinesterase activity. *Biochem. Pharmacol.* **1961**, *7*, 88-95.

(58) Baki, A.; Bielik, A.; Molnar, L.; Szendrei, G.; Keseru, G. M. A high throughput luminescent assay for glycogen synthase kinase-3 beta inhibitors. *Assay Drug Dev. Techn.* **2007**, *5*, 75-83.

(59) Cheung, J.; Rudolph, M. J.; Burshteyn, F.; Cassidy, M. S.; Gary, E. N.; Love, J.; Franklin, M. C.; Height, J. J. Structures of human acetylcholinesterase in complex with pharmacologically important ligands. *J. Med. Chem.* **2012**, *55*, 10282-10286.

(60) Saitoh, M.; Kunitomo, J.; Kimura, E.; Hayase, Y.; Kobayashi, H.; Uchiyama, N.; Kawamoto, T.; Tanaka, T.; Mol, C. D.; Dougan, D. R.; Textor, G. S.; Snell, G. P.; Itoh, F. Design, synthesis and structure-activity relationships of 1,3,4-oxadiazole derivatives as novel inhibitors of glycogen synthase kinase-3 beta. *Bioorg. Med. Chem.* **2009**, *17*, 2017-2029.

(61) Inestrosa, N. C.; Dinamarca, M. C.; Alvarez, A. Amyloid-cholinesterase interactions-implications for Alzheimer's disease. *FEBS J.* **2008**, *275*, 625-632.

(62) Rees, T.; Hammond, P. I.; Soreq, H.; Younkin, S.; Brimijoin, S. Acetylcholinesterase promotes beta-amyloid plaques in cerebral cortex. *Neurobiol. Aging* **2003**, *24*, 777-787.

Table of Contents Graphic